

This discussion paper is/has been under review for the journal Atmospheric Chemistry and Physics (ACP). Please refer to the corresponding final paper in ACP if available.

In situ secondary organic aerosol formation from ambient pine forest air using an oxidation flow reactor

B. B. Palm^{1,2}, P. Campuzano-Jost^{1,2}, A. M. Ortega^{1,3}, D. A. Day^{1,2}, L. Kaser^{4,5}, W. Jud⁵, T. Karl⁶, A. Hansel⁵, J. F. Hunter⁷, E. S. Cross⁷, J. H. Kroll^{7,8}, Z. Peng^{1,2}, W. H. Brune⁹, and J. L. Jimenez^{1,2}

¹Cooperative Institute for Research in Environmental Sciences, University of Colorado, Boulder, USA

²Department of Chemistry and Biochemistry, University of Colorado, Boulder, USA

³Department of Atmospheric and Oceanic Science, University of Colorado, Boulder, USA

⁴National Center for Atmospheric Research, Boulder, CO, USA

⁵Institute of Ion Physics and Applied Physics, University of Innsbruck, Innsbruck, Austria

⁶Institute of Meteorology and Geophysics, University of Innsbruck, Innsbruck, Austria

⁷Department of Civil and Environmental Engineering, Massachusetts Institute of Technology, Cambridge, MA, USA

⁸Department of Chemical Engineering, Massachusetts Institute of Technology, Cambridge, MA, USA

⁹Department of Meteorology, Pennsylvania State University, State College, PA, USA

Received: 6 October 2015 – Accepted: 13 October 2015 – Published: 4 November 2015

Correspondence to: J. L. Jimenez (jose.jimenez@colorado.edu)

Published by Copernicus Publications on behalf of the European Geosciences Union.

ACPD

15, 30409–30471, 2015

In situ secondary
organic aerosol
formation from
ambient pine forest
air

B. B. Palm et al.

[Title Page](#)

[Abstract](#)

[Introduction](#)

[Conclusions](#)

[References](#)

[Tables](#)

[Figures](#)

◀

▶

[Back](#)

[Close](#)

[Full Screen / Esc](#)

[Printer-friendly Version](#)

[Interactive Discussion](#)

Abstract

ACPD
15, 30409–30471, 2015

Ambient air was oxidized by OH radicals in an oxidation flow reactor (OFR) located in a montane pine forest during the BEACHON-RoMBAS campaign to study biogenic secondary organic aerosol (SOA) formation and aging. High OH concentrations and short residence times allowed for semi-continuous cycling through a large range of OH exposures ranging from hours to weeks of equivalent (eq.) atmospheric aging. A simple model is derived and used to account for the relative time scales of condensation of low volatility organic compounds (LVOCs) onto particles, condensational loss to the walls, and further reaction to produce volatile, non-condensing fragmentation products. More SOA production was observed in the OFR at nighttime (average $4 \mu\text{g m}^{-3}$ when LVOC fate corrected) compared to daytime (average $1 \mu\text{g m}^{-3}$ when LVOC fate corrected), with maximum formation observed at 0.4–1.5 eq. days of photochemical aging. SOA formation followed a similar diurnal pattern to monoterpenes, sesquiterpenes, and toluene + *p*-cymene concentrations, including a substantial increase just after sunrise at 07:00 LT. Higher photochemical aging (> 10 eq. days) led to a decrease in new SOA formation and a loss of preexisting OA due to heterogeneous oxidation followed by fragmentation and volatilization. When comparing two different commonly used methods of OH production in OFRs (OFR185 and OFR254), similar amounts of SOA formation were observed. We recommend the OFR185 mode for future forest studies. Concurrent gas-phase measurements of air after OH oxidation illustrate the decay of primary VOCs, production of small oxidized organic compounds, and net production at lower ages followed by net consumption of terpenoid oxidation products as photochemical age increased. New particle formation was observed in the reactor after oxidation, especially during times when precursor gas concentrations and SOA formation were largest. Approximately 6 times more SOA was formed in the reactor from OH oxidation than could be explained by the VOCs measured in ambient air. Several recently-developed instruments quantified ambient semi- and intermediate-volatility organic compounds (S/I VOCs) that were not detected by a PTR-TOF-MS. An SOA yield

Discussion Paper | Discussion Paper

ACPD

15, 30409–30471, 2015

In situ secondary organic aerosol formation from ambient pine forest air

B. B. Palm et al.

Title Page

Abstract

Introduction

Conclusions

References

Tables

Figures

◀

▶

Back

Close

Full Screen / Esc

Printer-friendly Version

Interactive Discussion



of 24–80 % from those compounds can explain the observed SOA, suggesting that these typically unmeasured S/IVOCs play a substantial role in ambient SOA formation. Our results allow ruling out condensation sticking coefficients much lower than 1. Our measurements help clarify the magnitude of SOA formation in forested environments, and demonstrate methods for interpretation of ambient OFR measurements.

1 Introduction

Atmospheric aerosols play a complex and important role in air pollution, human health, and global climate. Exposure to fine particles has adverse effects on cardiopulmonary health (Pope and Dockery, 2006). Aerosols affect climate forcing by directly scattering or absorbing incoming solar radiation. They also act as cloud condensation nuclei (CCN), affecting the reflectivity, lifetime, and precipitation of clouds (IPCC, 2013). Among all radiative forcings, the estimates for aerosols represent the largest uncertainty (Myhre et al., 2013).

Organic aerosols (OA) make up a substantial fraction of submicron aerosols (Murphy et al., 2006; Zhang et al., 2007; Jimenez et al., 2009). OA is composed of thousands of different molecules, of which only a small fraction has been speciated (Goldstein and Galbally, 2007). OA can be emitted directly in the particle phase as primary OA (POA), or it can be formed as secondary OA (SOA) through gas-to-particle conversion. During gas-phase SOA formation, an oxidant (mainly OH, O₃, or NO₃) reacts with organic gases to produce either less-volatile functionalization products (e.g., reacting to add a hydroxyl group) or more-volatile fragmentation products (e.g., breaking C-C bonds to produce smaller molecules). If the reaction products have sufficiently lower volatility, they can then partition into the particle phase to form SOA (Pankow, 1994; Donahue et al., 2006). In addition to gas-phase oxidation pathways, SOA formation can result from aqueous chemistry within aerosol water or in cloud droplets (e.g., Lim et al., 2010; Ervens et al., 2011; Ervens, 2015) or heterogeneous uptake reactions (e.g., Surratt et al., 2010). Oxidative aging of gases and particles continues until deposition

Title Page

Abstract

Introduction

Conclusions

References

Tables

Figures

|◀

▶|

◀

▶

Back

Close

Full Screen / Esc

Printer-friendly Version

Interactive Discussion



occurs (or CO₂ is produced). The complexity of OA chemistry arises from this intricate mix of multiphase-multigenerational reaction pathways and physicochemical processes involving thousands of molecules.

Much progress has been made in the past decade towards identifying and quantifying the sources, formation, and aging mechanisms of SOA. Aerosol models using traditional (pre-2007) aerosol yields for volatile organic compounds (VOCs) from chamber studies generally underpredict SOA mass by a factor of 10 in urban areas (Volkamer et al., 2006; Hodzic et al., 2010; Hayes et al., 2015). More recent models are able to better predict SOA mass in urban areas by adding previously ignored semivolatile and intermediate volatility organic compounds (S/IVOCs; Hodzic et al., 2010; Hayes et al., 2015). Recent measurements of the oxidation of biomass burning emissions, vehicle exhaust, and urban air have also found S/IVOCs to be important contributors to SOA formation (Grieshop et al., 2009; Miracolo et al., 2010; Zhao et al., 2014), building on the ideas of Robinson et al. (2007). However, model parameterizations of SOA formation from S/IVOCs are based on large extrapolations and are still uncertain. The recent AeroCom intercomparison of 31 global OA models showed large variability between models and low temporal correlations between models and measurements (Tsigaridis et al., 2014). Their work suggests that current model parameterizations of SOA formation, transport, and removal processes are inadequate.

SOA formation has traditionally been studied in large environmental “smog” chambers. These chamber experiments have provided the SOA yields for models, but recent evidence shows that chamber experiments are affected by large losses of semivolatile gases to chamber walls (Matsunaga and Ziemann, 2010; Zhang et al., 2014; Krechmer et al., 2015) in addition to well-known particle wall losses (Pierce et al., 2008). This is especially true at long (> 1 day) residence times, making it difficult to study SOA formation and aging on longer time scales. It is also difficult to perform field experiments with ambient air in smog chambers (Tanaka et al., 2003). To explore the sources of SOA on a rapid time scale and with a wide range of oxidant exposures, a variety of oxidation flow reactors (OFR) have been developed (Kang et al., 2007; George et al.,

In situ secondary organic aerosol formation from ambient pine forest air

B. B. Palm et al.

[Title Page](#)

[Abstract](#)

[Introduction](#)

[Conclusions](#)

[References](#)

[Tables](#)

[Figures](#)

[|◀](#)

[▶|](#)

[◀](#)

[▶](#)

[Back](#)

[Close](#)

[Full Screen / Esc](#)

[Printer-friendly Version](#)

[Interactive Discussion](#)

In situ secondary organic aerosol formation from ambient pine forest air

B. B. Palm et al.

[Title Page](#)[Abstract](#)[Introduction](#)[Conclusions](#)[References](#)[Tables](#)[Figures](#)[|◀](#)[▶|](#)[◀](#)[▶](#)[Back](#)[Close](#)[Full Screen / Esc](#)[Printer-friendly Version](#)[Interactive Discussion](#)

2 Experimental methods

2.1 BEACHON-RoMBAS campaign

The BEACHON-RoMBAS field campaign (Bio-hydro-atmosphere interactions of Energy, Aerosols, Carbon, H₂O, Organics and Nitrogen – Rocky Mountain Biogenic Aerosol Study; <http://cires.colorado.edu/jimenez-group/wiki/index.php/BEACHON-RoMBAS>) took place at the Manitou Experimental Forest Observatory near Woodland Park, Colorado, in July–August 2011 (39.10° N, 105.10° W; 2370 m elevation). It was a collaboration of 27 institutions from the United States and Europe, focused on understanding primary and secondary biogenic aerosol emissions, formation and processing. An overview of atmospheric chemistry research at the Manitou Experimental Forest Observatory, including the BEACHON-RoMBAS campaign, has been previously published (Ortega et al., 2014).

The sampling site was located in a ponderosa pine forest in a mountain valley. VOC concentrations were characterized by high 2-methyl-3-buten-2-ol (MBO) during the daytime and monoterpenes (MT) during the nighttime. VOCs at this site have been described in detail for previous campaigns during July–September 2008 (Kim et al., 2010) and August–September 2010 (Kaser et al., 2013a, b), while Fry et al. (2013) discussed diurnal cycles of select biogenic and anthropogenic VOCs during this campaign. The diurnal cycle of the concentration of MBO + isoprene (detected as the same product ion in the proton transfer reaction time-of-flight mass spectrometer; PTR-TOF-MS) measured at an above-canopy 25 m inlet ranged from about 1.5 ppb during the day to 0.3 ppb at night, while MT concentrations were on average 0.1 ppb during the day and 0.5 ppb at night. The relative ratio of isoprene/(MBO + isoprene) at this field site was estimated using GC-MS, PTR-TOF-MS, and whole air samples during summer 2010 (Kaser et al., 2013b) and using NO⁺ as a reagent ion during this campaign (Karl et al., 2012) to be approximately 20 %. Isoprene concentrations are calculated in this study using that approximation, which gives values typically < 300 ppt. While largely dominated by biogenic emissions, the site receives some airflow from the front

Title Page

Abstract

Introduction

Conclusions

References

Tables

Figures

◀

▶

Back

Close

Full Screen / Esc

Printer-friendly Version

Interactive Discussion



range urban areas (Denver metropolitan area and Colorado Springs) on most days, as evidenced by moderate increases in NO_x , CO, and anthropogenic VOCs during late afternoon and into the evening (Fry et al., 2013; Ortega et al., 2014; Chan et al., 2015).

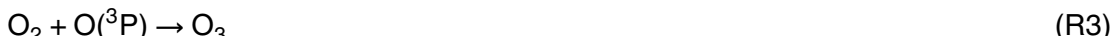
2.2 Oxidation flow reactor

- 5 The Potential Aerosol Mass (PAM) oxidation flow reactor (hereafter flow reactor or OFR) is a cylindrical tube 45.7 cm long and 19.7 cm ID with a volume of approximately 13 L, previously described elsewhere (Kang et al., 2007, 2011; Lambe et al., 2011a; Ortega et al., 2013, 2015). Ambient air was sampled through the reactor with a residence time of 2–4 min ($3.5\text{--}6.5 \text{ L min}^{-1}$ total flow rate), achieving oxidant exposures of hours
10 to months of eq. atmospheric aging. The inlet plate of the OFR was removed to reduce possible losses of semivolatile SOA precursors to the inlet plate inferred in a previous study (Ortega et al., 2013) and to reduce the width of the residence time distribution in the reactor. Air was sampled into the reactor through a 14 cm diameter coarse-grid mesh screen to reduce turbulence in the reactor and prevent insects and debris from
15 entering the reactor. The mesh was coated with an inert silicon coating (Sulfinert by SilcoTek, Bellefonte, PA) to minimize gas and particle losses. OH radicals in the OFR were produced inside the reactor through one of two methods: OH production from photolysis of ambient H_2O , O_2 , and concurrently produced O_3 using 185 and 254 nm light (referred to as the OFR185 method), or OH production from photolysis of injected
20 (externally produced) O_3 using 254 nm light (referred to as the OFR254 method; Peng et al., 2015a). O_3 and NO_3 oxidation were also investigated and will be the subject of a future manuscript.

For both methods, UV light was produced using two low-pressure mercury lamps (BHK, Inc., model no. 82-9304-03) mounted inside and on the upper part of the flow reactor. The lamps have discrete emission wavelengths of 185 and 254 nm. The fol-
25

Title Page	
Abstract	Introduction
Conclusions	References
Tables	Figures
◀	▶
◀	▶
Back	Close
Full Screen / Esc	
Printer-friendly Version	
Interactive Discussion	

lowing reactions produce the OH radicals:



In the OFR185 method, OH was produced by H_2O photolysis (Reaction 1) and also by O_3 photolysis (Reactions 4 and 5), as O_3 was formed in the reactor from O_2 photolysis (Reactions 2 and 3). In the OFR254 method, the mercury lamps were mounted inside Teflon-coated quartz sheaths, which blocked transmission of 185 nm light into the OFR, and only (Reactions 4 and 5) produced OH. Note that both wavelengths (185 and 254 nm) may initiate chemistry not normally occurring in the troposphere, and $\text{O}({}^3\text{P})$ and $\text{O}({}^1\text{D})$ are also present in the reactor at elevated concentrations. However, under the OFR conditions of our study neither of those non-OH reactants is a competitive reaction pathway (Peng et al., 2015b).

10 O_3 oxidation, on the other hand, can be competitive in the OH oxidation experiments under certain conditions. According to Fig. 5 of Peng et al. (2015b), O_3 in the OFR185 method during this study likely contributed only a minor (< 20 %) role in the oxidation of a few biogenic VOCs with largest $k_{\text{O}_3}/k_{\text{OH}}$ ratios, and only at the lowest OH exposures (OH_{exp}) equivalent to several hours of aging.

15 With the OFR254 method though, the ratio of O_3 exposure to OH_{exp} was as high as 10^6 for the lowest OH_{exp} in this study, meaning O_3 may have played a substantial role in the initial oxidation of a small number of biogenic VOCs under those conditions. Still, the relative importance of O_3 vs. OH oxidation in the OFR was over an order-of-magnitude lower than under typical daily-average atmospheric conditions (Peng et al., 2015b).

20 The OH exposure was stepped over a range of exposures by adjusting the mercury lamp intensities using programmable computer controls. A key parameter for interpreting the flow reactor aging was the total oxidant exposure, or oxidant concentration integrated over time, experienced by the sampled air. OH_{exp} for the OFR185 method

[Title Page](#)

[Abstract](#)

[Introduction](#)

[Conclusions](#)

[References](#)

[Tables](#)

[Figures](#)

◀

▶

[Back](#)

[Close](#)

[Full Screen / Esc](#)

[Printer-friendly Version](#)

[Interactive Discussion](#)



was estimated in part based on a model-derived equation, which uses measurements of ambient water vapor concentration, O_3 produced in the reactor, and estimated external OH reactivity (OHR_{ext}) as equation parameters (Li et al., 2015). To provide the best estimate of OH_{exp} for this study, the output OH_{exp} from the model was divided by a factor of two (which is within the estimated model uncertainty of a factor of three) in order to bring it into better agreement with VOC decay rates measured during this campaign (Sect. 3.2). OH_{exp} for the OFR254 method was calculated from a different model-derived equation, using OHR_{ext} and a measurement of the amount of O_3 consumed as equation parameters (Peng et al., 2015a), and was also divided by a factor of two. For both methods, OH_{exp} was converted to eq. days of atmospheric aging by dividing by a 24 h-average atmospheric concentration of $1.5 \times 10^6 \text{ molec cm}^{-3} OH$ (Mao et al., 2009). All usage of hours/days of aging in this work refers to eq. ages calculated in this manner.

Oxidant exposure is not the only factor that determines aerosol chemistry. NO_x concentrations have been shown to affect oxidation products and aerosol yields in chamber studies, especially due to the competition of NO and HO_2/RO_2 to react with the RO_2 radicals formed during oxidation (e.g., Ng et al., 2007; Lim and Ziemann, 2009). In all OH oxidation experiments in the reactor, ambient NO_x was rapidly oxidized to HNO_3 in as little as a couple of seconds at the highest OH concentrations, while photolysis of HNO_3 back to NO_x was too slow to compete with oxidation (Li et al., 2015). Thus, the OH flow reactor experiments were assumed to occur under $RO_2 + HO_2$ conditions.

2.3 Sampling strategy and measurements

An important advantage of the OFR technique is that the oxidant concentration inside the reactor can be rapidly and consistently controlled to achieve any desired amount of oxidation from hours up to many weeks of eq. atmospheric age. Stepping through a repeating cycle of several oxidant concentrations from no added OH to several weeks of eq. aging allowed continuous investigation of SOA formation as a function of this

In situ secondary organic aerosol formation from ambient pine forest air

B. B. Palm et al.

[Title Page](#)

[Abstract](#)

[Introduction](#)

[Conclusions](#)

[References](#)

[Tables](#)

[Figures](#)

◀

▶

[Back](#)

[Close](#)

[Full Screen / Esc](#)

[Printer-friendly Version](#)

[Interactive Discussion](#)



In situ secondary organic aerosol formation from ambient pine forest air

B. B. Palm et al.

[Title Page](#)

[Abstract](#)

[Introduction](#)

[Conclusions](#)

[References](#)

[Tables](#)

[Figures](#)

[|◀](#)

[▶|](#)

[◀](#)

[▶](#)

[Back](#)

[Close](#)

[Full Screen / Esc](#)

[Printer-friendly Version](#)

[Interactive Discussion](#)

age. The time needed to complete one cycle was kept as short as possible (~2 h), limited by the number of steps and reactor residence time. This allows SOA formation to be studied over the whole range of exposures as functions of time of day and the concentration of precursors that change on that time scale.

In typical OFR185 and OFR254 exposure cycles during BEACHON-RoMBAS, the UV lamps inside the reactor were stepped through six 20 min-long settings of varying lamp intensities for a combined cycle length of 2 h, from both lamps off to both lamps at full intensity. Oxidant and product concentrations in the reactor were allowed 15 min (~4–7 reactor residence times) to reach a steady state at each light setting (mainly to allow the OFR to flush, as the lamp UV intensity stabilizes within seconds) before being sampled for the last 5 min of each cycle. Immediately after this 5 min sampling period, the lamp intensity was changed to prepare for the next oxidant concentration in the cycle. During the 15 min in which the OFR was not being sampled, ambient aerosols were sampled directly, through a thermodenuder (Huffman et al., 2008), and directly again, for 5 min each. In this method, all perturbation measurements (OFR or thermodenuder) are bracketed by unperturbed ambient measurements. The ambient AMS sampling has also been described in Fry et al. (2013).

Ambient aerosols and those after oxidation in the OFR were measured using a TSI 3936 Scanning Particle Mobility Analyzer (SMPS) and an Aerodyne High-Resolution Time-of-Flight Aerosol Mass Spectrometer (HR-ToF-AMS, hereafter AMS; DeCarlo et al., 2006). A system of automated valves (Aerodyne AutoValve), controlled by a custom automation program written in Labview (National Instruments, Inc.), was used to multiplex the AMS and SMPS to alternate between measuring ambient air and air oxidized in the OFR (or heated by the thermodenuder). The flow rate through the OFR and all sampling lines was kept constant at all times by using make-up flows when not sampling from each of the inlet lines or reactors. The same custom software was used to control and schedule the UV lamp cycling as well as record RH, temperature and output O₃ concentrations in the OFR. Sampled air was dried to < 30 % relative humidity upstream of the SMPS and AMS using a Nafion membrane drier (Perma Pure,

LLC; MD-110-24S-4). For OH_{exp} calculations in the OFR, O₃ was measured using a 2B Technologies Model 205 Monitor and ambient water vapor was measured using a Vaisala HM70 probe. A schematic of the experimental setup is shown in Fig. 1. The SMPS consisted of a TSI 3080 Electrostatic Classifier, a 3081 long Differential Mobility Analyzer (DMA) column, and a 3010 Condensation Particle Counter (CPC). It was operated with sheath and aerosol flow rates of 3.0 and 0.3 L min⁻¹, respectively, with a TSI Kr-85 neutralizer and no impactor. The SMPS sampled the range of 14–626 nm mobility diameters, with one 4 min scan every five minutes, and synchronized with OFR and AMS sampling.

The AMS data used in this analysis was recorded as 2.5 min average mass spectra in "V-mode". Instrument sensitivity was calibrated every 3 days with 400 nm monodisperse, dried, ammonium nitrate particles. The gas-phase N₂ signal, commonly referred to as the airbeam, was used to track changes in sensitivity between calibrations. The flow rate of air into the AMS was calibrated in the field before measurements began. A fluorocarbon standard was leaked into the ionization chamber in order to provide high *m/z* background peaks for improved *m/z* calibration up to approximately *m/z* 300 (DeCarlo et al., 2006). Corrections were applied to account for gas-phase CO₂ interference and water fragmentation patterns using daily aerosol-free background filters and continuous ambient CO₂ measurements. AMS and SMPS concentrations and SMPS size distributions were corrected to account for diffusion losses to the walls of the inlet sampling lines, described in Sect. S1 in the Supplement. AMS data was processed using a collection efficiency (CE) of 1, detailed in Sect. S2 and based on a comparison of the AMS and SMPS measurements of ambient aerosol volume (Fig. S2), OFR-oxidized aerosol volume and volume added (Fig. S3), and total volume enhancement as a function of photochemical age (Fig. S4). AMS concentrations were also corrected for losses of small particles through the aerodynamic lens and to the OFR walls. Details for these corrections can be found in the Sect. S3. AMS data is reported at 293 K and 0.76 atm (typical ambient values at this research site). The time series, diurnal cycles, and average size distributions of ambient OA, sulfate (SO₄), nitrate (NO₃), and am-

In situ secondary organic aerosol formation from ambient pine forest air

B. B. Palm et al.

[Title Page](#)

[Abstract](#)

[Introduction](#)

[Conclusions](#)

[References](#)

[Tables](#)

[Figures](#)

[|◀](#)

[▶|](#)

[◀](#)

[▶](#)

[Back](#)

[Close](#)

[Full Screen / Esc](#)

[Printer-friendly Version](#)

[Interactive Discussion](#)



monium (NH_4) aerosol mass concentrations have been previously published (Ortega et al., 2014).

While both OH generation methods detailed above were used during the campaign, the analysis in this paper will mainly focus on the OFR185 mode for several reasons.

- 5 Determination of ages below approximately 1 eq. day using the OFR254 method was limited by the ability to accurately measure the amount of injected O_3 that was consumed in the reactor. The variability of the measurement of the initial concentration of O_3 inside the reactor was approximately $\pm 2 \text{ ppm}$ (when reaching a total of about 70 ppm of O_3) due to variations in the mixing of injected O_3 with ambient air sampled into the OFR, especially when sampling in windy conditions. The model used to estimate eq. age for the OFR254 method estimated that 2 ppm of photolyzed O_3 produced an age of 0.5 eq. days, so that was the effective lower limit of detection of age with the OFR254 method under the experimental conditions used during this campaign. Also, the OFR254 method requires high concentrations of O_3 (up to 70 ppm in this study) 10 to be injected in order to reach high ages. As discussed above, O_3 may play a role in the oxidation of some VOCs in the OFR254 method, while the role of O_3 oxidation in OFR185 is minor. This could further complicate the interpretation of the results of OH oxidation for the lower measurable ages (hours–days) when using OFR254. In addition, the temporal data coverage of OFR185 oxidation (23 July–4 August, 9–14 and 15 20 24–26 August) was much greater than OFR254 (17–20 and 28–30 August). Regardless, we document below that both OH oxidation methods gave consistent results for SOA production (Sect. 3.4). For these reasons OFR254 data was not included in the rest of the analyses. The time series of OFR185 and OFR254 OA measurements are shown compared to ambient OA and MT in Fig. S7.

25 This work focuses on the changes in OA mass due to SOA formation and OA aging as a result of exposure of ambient air to OH. OA enhancement is defined here as the difference between OA mass measured by the AMS after oxidation in the OFR and the average of the two ambient OA concentrations measured just before and after the oxidation data point. If SOA was produced in the reactor, the OA enhancement was

In situ secondary organic aerosol formation from ambient pine forest air

B. B. Palm et al.

[Title Page](#)

[Abstract](#)

[Introduction](#)

[Conclusions](#)

[References](#)

[Tables](#)

[Figures](#)

[|◀](#)

[▶|](#)

[Back](#)

[Close](#)

[Full Screen / Esc](#)

[Printer-friendly Version](#)

[Interactive Discussion](#)



positive; if oxidation led to a net loss of OA mass, then the OA enhancement was negative. As discussed in the results below, SOA formation in the OFR correlated with ambient precursor gas concentrations. If the ambient concentration of those gases was close to zero, then no SOA formation was observed (e.g., Fig. 8). Therefore, any SOA formation from, e.g., gases desorbing from the OFR walls, was negligible.

Measurements of VOCs in ambient air and after OFR oxidation were made using a high-resolution PTR-TOF-MS (Kaser et al., 2013b). This technique can separate and identify isobaric compounds with a mass resolution ($m/\Delta m$) of up to ~ 4000 . This allowed for tracking of the depletion of primary biogenic species in the OFR as well as the production of more oxygenated products. Signals from isotopes, internal standards, and possible artifacts (e.g., saturated hydrocarbons that correlate with O_3 concentration in the reactor) were removed from the analysis. When calculating predicted depletion for α -pinene, β -pinene, 3-carene, toluene, *p*-cymene, methanol, and sesquiterpenes (SQT; using longifolene as a representative compound) in the following analysis, the rate constants used were: $k_{OH} = 5.3 \times 10^{-11}$, 7.7×10^{-11} , 8.7×10^{-11} , 5.5×10^{-12} , 1.5×10^{-11} , 9.1×10^{-13} , and $4.8 \times 10^{-11} \text{ cm}^3 \text{ molec}^{-1} \text{ s}^{-1}$, respectively (Calvert et al., 2002; Atkinson and Arey, 2003; Alarcón et al., 2014). As an approximation of previous measurements at this site, MT are assumed to be an equal mix of α -pinene, β -pinene, and 3-carene for this analysis (Kim et al., 2010; Ortega et al., 2014). Likewise, the ratio of toluene : *p*-cymene used in calculations was taken from Kaser et al. (2013b) to be 74 : 26. Similar to the multiplexing scheme described above for particle sampling, a system of automated Teflon valves was used to alternate between measuring ambient air and air through the OFR, sampling from the OFR concurrently with the AMS + SMPS. PTR-TOF-MS measurements from the OFR were performed during 1–4 and 24–25 August 2011, while using the OFR185 method. The analysis here focuses on two consecutive sampling cycles from 00:00–04:00 MDT (LT) on 3 August 2011, when the concentration of MT was relatively high (0.8 ppbv) and the concentration of MBO + isoprene was relatively low (0.1 ppbv).

5

10

15

20

25

In situ secondary organic aerosol formation from ambient pine forest air

B. B. Palm et al.

[Title Page](#)[Abstract](#)[Introduction](#)[Conclusions](#)[References](#)[Tables](#)[Figures](#)[|◀](#)[▶|](#)[Back](#)[Close](#)[Full Screen / Esc](#)[Printer-friendly Version](#)[Interactive Discussion](#)

Ambient PTR-TOF-MS measurements are also used in this work to estimate how much SOA could form in the OFR. The continuous PTR-TOF-MS measurements during BEACHON-RoMBAS were made from an inlet at the top of a tower above the canopy at 25 m height, while the OFR was located on top of an instrument trailer within the canopy at approximately 4 m height. In-canopy gradients were accounted for by comparing the PTR-TOF-MS measurements at 25 m with measurements made through the OFR in the absence of oxidant and with measurements from a different nearby inlet at 1 m height. It was observed that the concentrations of MT, SQT, MBO + isoprene, and toluene + *p*-cymene were approximately 1.9, 5.9, 1.4, and 1.2 times higher in the canopy than at 25 m, respectively (discussed in Sect. S4). All analyses in this work were done using estimated in-canopy concentrations, which were inferred by applying these empirical relationships to the continuous 25 m inlet measurements. This scaling technique has been used before, producing similar results when applied to measurements during the summer 2010 BEACHON-ROCS campaign at the same field location (Kim et al., 2013; Wolfe et al., 2014).

Ambient SO₂ concentrations were measured using a Thermo Environmental Model 43C-TLE analyzer. Data were reported as 5 min averages from 6 different heights on a tower up to 25.1 m. We used only data measured at the 5 m height, to best match the height of the OFR on top of the trailer. The SO₂ instrument was automatically zeroed every 6 h, using scrubbed zero grade air. It was calibrated by a standard addition of 3 sccm of a 14 ppmv SO₂ in N₂ standard (Scott–Marrin) into the 3 slpm sample flow.

A novel thermal desorption electron impact mass spectrometer (TD-EIMS) was used to measure ambient concentrations of ensemble S/I VOCs with volatilities in the range of effective saturation vapor concentrations (C^*) of 10^1 – 10^7 µgm^{−3}. This method involved cryogenic collection of organic gases, temperature-programmed desorption into ultra-high-purity (UHP) helium, and measurement with a high-resolution time-of-flight mass spectrometer (Cross et al., 2013; Hunter et al., 2015). The TD-EIMS provided a time series of the gas-phase organic mass and composition in each volatility bin.

In situ secondary organic aerosol formation from ambient pine forest air

B. B. Palm et al.

[Title Page](#)

[Abstract](#)

[Introduction](#)

[Conclusions](#)

[References](#)

[Tables](#)

[Figures](#)

◀

▶

◀

▶

[Back](#)

[Close](#)

[Full Screen / Esc](#)

[Printer-friendly Version](#)

[Interactive Discussion](#)

3 Results and discussion

3.1 OFR operation

Typical OFR operation using the OFR185 method is illustrated in Fig. 2, by an example of the evolution of OA and SO₄ aerosol mass concentrations as OH concentration was cycled through the range of eq. ages. As age increased over the first few lamp settings, OA mass increased due to production and condensation of low volatility species from the oxidation of gas-phase SOA precursors. SO₄ mass remained nearly the same as in ambient air for these lower ages. The increase of SOA mass at lower ages compared to SO₄ is thought to be due to the different rate constants for reaction of OH. The rates with biogenic VOCs, e.g., $k_{\text{OH}} = 5.3 \times 10^{-11} \text{ cm}^3 \text{ molec}^{-1} \text{ s}^{-1}$ for α -pinene (Atkinson and Arey, 2003), are generally much faster than the reaction of OH with SO₂, where $k_{\text{OH}} = 9.49 \times 10^{-13} \text{ cm}^3 \text{ molec}^{-1} \text{ s}^{-1}$ (Sander et al., 2011). As the eq. age continued to increase, OA mass enhancement decreased, eventually resulting in net OA loss, while SO₄ mass continued to increase. This high eq. age led to lack of formation of SOA as well as heterogeneous oxidation of the preexisting OA, leading to fragmentation and evaporation (Ortega et al., 2015). As expected, SO₄ aerosol was not consumed in this way by excess OH_{exp}.

3.2 VOC enhancement/depletion vs. eq. age

VOCs were measured before (in ambient air) and after OH oxidation in the OFR using a PTR-TOF-MS. This showed which VOCs were being depleted, potentially to form SOA, as well as which products were being formed. Also, the decay of VOCs after oxidation provided a direct measurement for validation of the model-derived age estimates. A number of likely compounds have been identified based on measurements from previous campaigns at the Manitou Experimental Forest Observatory site (Kim et al., 2010; Kaser et al., 2013a), as listed in Table 1.

[Title Page](#)[Abstract](#)[Introduction](#)[Conclusions](#)[References](#)[Tables](#)[Figures](#)[|◀](#)[▶|](#)[◀](#)[▶](#)[Back](#)[Close](#)[Full Screen / Esc](#)[Printer-friendly Version](#)[Interactive Discussion](#)

For an overview of PTR-TOF-MS measurements, the difference mass spectrum and mass defect (exact mass minus nominal mass) plots for 4 eq. h of aging during nighttime are shown in Fig. 3. The greatest absolute magnitude of depletion in oxidized air compared to ambient nighttime air was observed for MT. Depletion was also observed for toluene + *p*-cymene, MBO + isoprene, SQT, pinonaldehyde + caronaldehyde, and camphor + α -pinene oxide. Notably, formation of nopinone was observed after 4 eq. h of aging. OH oxidation also led to substantial production of several relatively small oxidation product molecules, including formaldehyde, acetaldehyde, formic acid, acetone, and acetic acid, which have been commonly observed in similar photooxidation experiments (e.g., Lee et al., 2006; Ortega et al., 2013). Many other unidentified molecules were observed to be produced in smaller concentrations as a result of OH oxidation in the flow reactor. A similar plot is shown for higher eq. age (7 days) in Fig. S9, for comparison to Fig. 3. At such a high age, species such as MT, SQT, and toluene + *p*-cymene were completely depleted, while many small oxidation products increased as much as 5-fold.

In general for all degrees of oxidation, molecules with higher positive mass defects (corresponding to more chemically reduced species such as hydrocarbons) were depleted. Conversely, molecules with lower mass defect (more oxygenated compounds) were formed. This trend is consistent with what would be expected from gas-phase or heterogeneous OH oxidation chemistry. Also, Fig. 3 shows that monoterpenes constituted the majority of VOCs measured by the PTR-TOF-MS that were depleted after oxidation, while other compounds associated with terpenoid emissions and/or oxidation products were consumed or produced in smaller concentrations.

The relative changes of each of the compounds discussed above are shown as a function of OH_{exp} in Fig. 4. As previously discussed, nopinone is an example of a compound that increased in concentration at 4 h eq. age, indicating that it was an oxidation product in the OFR. This signal showed net formation at low ages (earlier than the peak of maximum SOA formation in the OFR) and eventually decreased to net loss at high exposures, as expected due to its reactivity with OH. Figure 4 also shows

In situ secondary organic aerosol formation from ambient pine forest air

B. B. Palm et al.

[Title Page](#)

[Abstract](#)

[Introduction](#)

[Conclusions](#)

[References](#)

[Tables](#)

[Figures](#)

[|◀](#)

[▶|](#)

[◀](#)

[▶](#)

[Back](#)

[Close](#)

[Full Screen / Esc](#)

[Printer-friendly Version](#)

[Interactive Discussion](#)

In situ secondary organic aerosol formation from ambient pine forest air

B. B. Palm et al.

[Title Page](#)[Abstract](#)[Introduction](#)[Conclusions](#)[References](#)[Tables](#)[Figures](#)[|◀](#)[▶|](#)[◀](#)[▶](#)[Back](#)[Close](#)[Full Screen / Esc](#)[Printer-friendly Version](#)[Interactive Discussion](#)

the net decay of several other terpene-related species and the formation of smaller, more volatile oxidation products as OH_{exp} increased. While the MBO + isoprene signal showed a substantial increase with increasing age, this is likely due to production of an isomeric interference, e.g., a fragment of an oxidation product.

- An assessment of the accuracy of the model-derived OH_{exp} (including the factor of two decrease discussed in Sect. 2.2) can be made by comparing the measured depletion of gases vs. expected depletion using published reaction rates with OH. This comparison is shown for an average speciated MT mixture, toluene + *p*-cymene, and methanol in Fig. 4. The MT and methanol signals decay slower than predicted, while the toluene + *p*-cymene signal decays slightly faster. These results are consistent with the previous evaluation of the model-predicted OH_{exp} for laboratory and field studies (Li et al., 2015). Determination of OH_{exp} in the OFR is limited by many factors, including model uncertainties (Peng et al., 2015a), the true non-plug-flow residence time distribution in the OFR, the difficulty of measuring a difference of signals using the PTR-TOF-MS in a perturbed environment, the possibility of competing production of the measured compounds (e.g., methanol), interferences and/or false identification of measured signal (e.g., fragments or different species with the same elemental composition interfering with the measured ions), and uncertainty in the relative composition of the MT and toluene + *p*-cymene mixtures. Despite these uncertainties, the PTR-TOF-MS is clearly measuring formation and decay of compounds that react with OH on the time scale of several hours of photochemical age. This is strong evidence that the OFR can be used to study a wide range of atmospherically-relevant time scales.

3.3 Fate of condensable gases in an OFR

3.3.1 Modeled low-volatility organic compound (LVOC) fate

- In order to properly interpret SOA formation as a function of age in an OFR, the time scales of various competing processes need to be carefully considered in the context of the relative importance of those processes in the OFR vs. the atmosphere. When

organic gases are oxidized in the OFR, they can form LVOCs, a term used here to describe organic gases with volatilities that are low enough to condense onto particles or surfaces. In the atmosphere, the dominant fate of these LVOCs is to condense onto aerosols, as dry and wet deposition are slower sinks (Knote et al., 2015; Nguyen et al., 2015). However, due to the different time scales, the LVOCs formed in the OFR can have other fates besides condensation onto aerosols. These include condensational loss to the walls of the OFR, further reaction with OH to produce either condensable or non-condensable gas-phase products, or exiting the reactor in the gas-phase (where they will almost entirely condense on the sampling tube walls, due to the large surface-area-to-volume ratio). If the LVOCs condense onto aerosols, then they are measured by the AMS + SMPS. However, if they are subject to one of the other three fates, then the AMS + SMPS measurements would underestimate the amount of SOA that would form in the atmosphere at the same level of OH exposure, and a correction is needed. Note that this section pertains to gas-phase losses, while a correction for particle losses to the OFR walls was also included as described in Sect. S3. The need for an LVOC correction to OFR measurements has been suggested before (Lambe et al., 2011a, 2015), but to our knowledge this work is the first attempt to apply one.

In this analysis, we calculate approximate lifetimes of LVOCs for condensation onto aerosols (τ_{aer}), loss to the walls of the OFR (τ_{wall}), and reaction with OH (τ_{OH}) as a function of OH_{exp} . Some semivolatile species (SVOC) will also be produced. However, we focus on LVOCs for simplicity, and also based on the observation that most of the OA has low volatility at this site, according to thermal denuder measurements (Hunter et al., 2015), and consistent with measurements at other locations (Cappa and Jimenez, 2010; Lopez-Hilfiker et al., 2015).

– τ_{aer} : following Pirjola et al. (1999), the lifetime for LVOC condensation onto aerosols was calculated as

$$\tau_{\text{aer}} = \frac{1}{4\pi \cdot \text{CS} \cdot D} \quad (1)$$

In situ secondary organic aerosol formation from ambient pine forest air

B. B. Palm et al.

[Title Page](#)

[Abstract](#)

[Introduction](#)

[Conclusions](#)

[References](#)

[Tables](#)

[Figures](#)

[|◀](#)

[▶|](#)

[Back](#)

[Close](#)

[Full Screen / Esc](#)

[Printer-friendly Version](#)

[Interactive Discussion](#)

with a diffusion coefficient $D = 7 \times 10^{-6} \text{ m}^2 \text{ s}^{-1}$ representative of an oxidized organic molecule with a molecular weight of approximately 200 g mol^{-1} at the field site ambient pressure (Tang et al., 2015). CS is the “condensational sink”

$$\text{CS} = \int_0^\infty r \beta(r) N(r) dr \quad (2)$$

which is the integral of the first moment of the particle size distribution, where r is particle radius, $N(r)$ is the particle number size distribution, and

$$\beta(r) = \frac{Kn + 1}{0.377Kn + 1 + \frac{4}{3}\alpha^{-1}Kn^2 + \frac{4}{3}\alpha^{-1}Kn} \quad (3)$$

is the Fuchs–Sutugin correction for gas diffusion to a particle surface in the transition regime, calculated using the sticking coefficient α of the condensing species (Seinfeld and Pandis, 2006). CS was calculated using the average of the SMPS size distributions of ambient air entering the OFR and of air exiting the OFR after oxidation, as a best approximation of the actual CS experienced by LVOCS in the OFR. The correction $\beta(r)$ is a function of the Knudsen number

$$Kn = \frac{\lambda_g}{r} \quad (4)$$

where λ_g is the mean free path of the condensing gas. Based on previous modeling and measurements, we assume $\alpha = 1$ for LVOCS (Kulmala and Wagner, 2001; Julin et al., 2014; Krechmer et al., 2015). A sensitivity study on the values of D , the impact of deviations from $\alpha = 1$, and the choice of SMPS size distribution used to calculate CS is discussed below in Sect. 3.6.3.

Title Page

Abstract

Introduction

Conclusions

References

Tables

Figures

|◀

▶|

◀

▶

Back

Close

Full Screen / Esc

Printer-friendly Version

Interactive Discussion

- τ_{wall} : following McMurry and Grosjean (1985), we estimate the first-order rate of LVOCS loss to the walls of the OFR limited by eddy diffusion as

$$k_{\text{wall}} = \frac{1}{\tau_{\text{wall}}} = \frac{A}{V} \cdot \frac{2}{\pi} \cdot \sqrt{k_e D} \quad (5)$$

We used the measured OFR surface-area-to-volume ratio of $A/V = 25 \text{ m}^{-1}$ and a coefficient of eddy diffusion $k_e = 0.0036 \text{ s}^{-1}$ (much faster than the coefficient D estimated above), estimated by extrapolating values given in McMurry and Grosjean (1985). The choice of k_e is included in the sensitivity analysis in Sect. 3.6.3. Equation (5) results in an estimated wall loss rate of 0.0025 s^{-1} ($\tau_{\text{wall}} = 400 \text{ s}$), similar to the lifetime of $\sim 600 \text{ s}$ estimated for this type of OFR in Lambe et al. (2011a). In the absence of any CS and oxidant, an upper limit of approximately 30 % of LVOCS would be lost to the walls and the balance would exit the reactor and be lost to the tubing walls. When including this campaign's average integrated particle surface area of $63 \mu\text{m cm}^{-3}$ (with number mode at $\sim 50 \text{ nm}$) in the calculation, the percentage lost to the walls decreases by only a few percent to 26 %. If using an integrated particle surface area of $500 \mu\text{m cm}^{-3}$ that might be found in an urban, pollution source, or lab study, the percentage drops to 15 %.

- τ_{OH} : to estimate the loss of LVOCS to non-condensable products due to continued reaction with OH, τ_{OH} , we make the assumption that LVOCS will remain available to condense on aerosols, walls, or exit the reactor for up to 5 generations of OH reaction. After they have reacted 5 times with OH, they are deemed lost by fragmentation into small oxidized molecules that are too volatile to condense. Further, we assume a rate constant for reaction with OH (of the order of that for an oxygenated molecule with ten carbon atoms and no C=C double bonds) of $k_{\text{OH}} = 1 \times 10^{-11} \text{ cm}^3 \text{ molec}^{-1} \text{ s}^{-1}$ (Ziemann and Atkinson, 2012), so

$$\tau_{\text{OH}} = \frac{5}{k_{\text{OH}} \cdot [\text{OH}]} \quad (6)$$

[Title Page](#)[Abstract](#)[Introduction](#)[Conclusions](#)[References](#)[Tables](#)[Figures](#)[|◀](#)[▶|](#)[◀](#)[▶|](#)[Back](#)[Close](#)[Full Screen / Esc](#)[Printer-friendly Version](#)[Interactive Discussion](#)

Sensitivity studies for variations in parameters k_{OH} and the number of reactions with OH before LVOCs fragment to non-condensable products are also discussed in Sect. 3.6.3.

These three lifetimes are combined to determine the total lifetime of loss of LVOCs to these three combined pathways,

$$\tau_{\text{total}} = \left(\frac{1}{\tau_{\text{aer}}} + \frac{1}{\tau_{\text{wall}}} + \frac{1}{\tau_{\text{OH}}} \right)^{-1} \quad (7)$$

This total lifetime is compared to the average OFR residence time τ_{OFR} (OFR volume divided by flow rate) to determine the fraction of LVOCs that exits the OFR without reaching one of the three other fates (and thus condenses onto sampling line walls),

$$F_{\text{exit}} = e^{-\frac{\tau_{\text{OFR}}}{\tau_{\text{total}}}} \quad (8)$$

The fraction of LVOCs that is lost to each pathway inside the OFR is then

$$F_x = (1 - F_{\text{exit}}) \cdot \left(\frac{k_x}{k_{\text{total}}} \right) \quad (9)$$

where the rate constant $k_x = \tau_x^{-1}$ and $x = \text{wall}, \text{OH}, \text{or aerosol (aer)}$.

Figure 5c compares all of the LVOC lifetimes and fractional fates as a function of age and OH_{exp} , with a typical OFR residence time of 140 s shown for comparison. The fractional fates are shown using high (Fig. 5a) and low (Fig. 5b) rates of condensation to aerosol, based on typical higher and lower aerosol surface areas during this particular campaign. As discussed below (Sect. 3.5), OH oxidation leads to a substantial increase in the number of small particles when gas-phase precursors are available. This in turn increases the surface area available for condensation of LVOCs, and therefore τ_{aer} depends on the amount of SOA formed from OH oxidation in the OFR in addition to the ambient particle surface area. During times of low SOA formation ($< 0.3 \mu\text{g m}^{-3}$), total surface area concentrations after oxidation are similar to ambient concentrations in the

Title Page

Abstract

Introduction

Conclusions

References

Tables

Figures

|◀

▶|

◀

▶|

Back

Close

Full Screen / Esc

Printer-friendly Version

Interactive Discussion

In situ secondary organic aerosol formation from ambient pine forest air

B. B. Palm et al.

[Title Page](#)[Abstract](#)[Introduction](#)[Conclusions](#)[References](#)[Tables](#)[Figures](#)[|◀](#)[▶|](#)[◀](#)[▶](#)[Back](#)[Close](#)[Full Screen / Esc](#)[Printer-friendly Version](#)[Interactive Discussion](#)

range of $30\text{--}100 \mu\text{m}^2 \text{cm}^{-3}$, and τ_{aer} is estimated to be approximately 400 s or longer. However, during times with $> 1.5 \mu\text{g m}^{-3}$ SOA formation, total surface area concentrations increase to $100\text{--}400 \mu\text{m}^2 \text{cm}^{-3}$ or larger and τ_{aer} becomes < 100 s.

- For an eq. age of 0.1 day, as little as 20 % of the LVOCs formed in the OFR are predicted to condense onto aerosols, with the rest being lost to the walls in or after the OFR. However, the majority of LVOCs are likely not produced until higher OH_{exp} , concurrent with the highest SOA production. As eq. age increases into the 0.2–3 day range, condensation onto aerosols can account for as much as 60 % of LVOC fate, provided there is enough SOA formation to sufficiently increase the total particle surface area.
- In this case, shown in Fig. 5a, the remaining 40 % of LVOCs are approximately equally split between loss to the walls, exiting the OFR, and reacting with $\text{OH} > 5$ times. However if sufficient particle surface area is not formed, as in Fig. 5b, then still only 20 % of LVOCs will condense onto aerosols.

For the conditions analyzed here from the BEACHON-RoMBAS campaign, these calculations suggest that when there were enough gas-phase precursors to produce $> 1.5 \mu\text{g m}^{-3}$ SOA, it is likely that the majority of this aerosol (up to ~ 60 %) would be produced and measured in the OFR despite the perturbed time scales. When there were relatively few gas-phase precursors and little SOA was formed, it is likely that a majority of the LVOCs were not able to condense into SOA during the reactor residence time. However, if there were few precursors to begin with, the absolute amount of potential SOA mass that would not have time to condense would still be relatively small, limiting the effect of this correction on the objectives of this study.

Another important conclusion from this analysis is that for high eq. ages > 10 days, a very small fraction of the LVOC formed (< 10 %) will condense to form new SOA. The remainder will react many times with OH before having a chance to condense, likely leading to smaller fragmentation products that are too volatile to condense into SOA. This is, of course, different from what occurs in the atmosphere, where LVOCs would typically have sufficient time for condensation to aerosols under most conditions. Since this rapid oxidation will remove any semi-volatile vapors from the gas phase, semi-

volatile OA molecules will begin to evaporate to reestablish equilibrium partitioning. However, measurements of evaporation kinetics for ambient and lab-generated SOA suggest that evaporation is too slow to account for the changes measured during the short OFR residence time (Vaden et al., 2011). Furthermore, thermodenuder measurements have shown that only a small fraction (~ 20 %) of ambient OA would be susceptible to evaporation due to removal of the gas phase molecules (Cappa and Jimenez, 2010; Ortega et al., 2015). Therefore, heterogeneous oxidation of the preexisting OA by OH likely dominates the measured OA depletion at very high eq. ages (DeCarlo et al., 2008; Ortega et al., 2015).

10 3.3.2 Model validation: sulfuric acid (H_2SO_4) condensation

To validate this LVOC fate model, we use the analogous and simpler system of oxidation of SO_2 by OH to form H_2SO_4 . If the H_2SO_4 condenses onto aerosols, it will be measured as SO_4 aerosol by the AMS. SO_4 aerosol formation in the OFR was predicted by using estimated OH_{exp} to calculate how much ambient SO_2 would be oxidized into H_2SO_4 . The LVOC fate model was then used to determine F_{aer} , F_{wall} , and F_{exit} for H_2SO_4 , while F_{OH} was set equal to zero since gas-phase H_2SO_4 will not continue to react with OH to produce volatile fragments. We used $D = 1 \times 10^{-5} \text{ m}^2 \text{ s}^{-1}$ for an H_2SO_4 molecule hydrated by H_2O molecules in the gas phase at the relevant ambient pressure and humidity (Hanson and Eisele, 2000), and the best-fit value of $\alpha = 0.65$ from Pöschl et al. (1998). An additional minor correction was applied to account for the fact that the $\text{SO}_2 + \text{OH}$ reaction is relatively slow, so the effective τ_{OFR} for H_2SO_4 molecules in the reactor can be less than the full OFR residence time depending on OH_{exp} . Using the model results, the fraction of H_2SO_4 that does not condense onto aerosol was corrected for by dividing the SO_4 mass measured with the AMS by F_{aer} .

The measured vs. predicted SO_4 enhancement after OH oxidation in the OFR using the OFR185 method is shown in Fig. 6. The AMS measured 61 % of the predicted SO_4 enhancement. After applying the correction, the measured and predicted SO_4 en-

Title Page	
Abstract	Introduction
Conclusions	References
Tables	Figures
◀	▶
◀	▶
Back	Close
Full Screen / Esc	
Printer-friendly Version	
Interactive Discussion	

hancements agreed well with a slope of 0.89, and R^2 slightly increased from 0.80 to 0.84. To illustrate the sensitivities of this model to key uncertain parameters, namely the effects of using the range of $\alpha = 0.43\text{--}1$ given in Pöschl et al. (1998) and using the SMPS size distributions measured before or after oxidation in the OFR (as lower and upper bounds of CS) are illustrated in Fig. S10. The amount of SO_4 formed was consistent with the expected amount within the uncertainties. This analysis demonstrates that a correction can be successfully applied for H_2SO_4 condensation, and that a similar correction should also be applied for LVOC condensation to accurately interpret the results of SOA formation in an OFR.

In the subsequent analyses, SOA formation is presented both with and without applying a correction to account for incomplete LVOC condensation to aerosol in the reactor. The correction, hereafter referred to as the “LVOC fate correction,” is applied by dividing the amount of SOA mass formed by F_{aer} . The correction is only applied for data with eq. age < 5 days. At higher exposures, it becomes unfeasible to apply the correction, because dividing small SOA mass formation by small fractions of condensation on aerosol results in large uncertainties. Instead, only uncorrected data is shown for eq. age > 5 days, and it is interpreted as being dominated by heterogeneous oxidation.

3.4 SOA mass enhancement vs. OH_{exp}

Both the concentrations and relative fractions of ambient SOA precursor gases changed between day and night. They were dominated by MBO + isoprene (under ambient OH chemistry) during the day, and by MT + SQT (under ambient O_3/NO_3 chemistry) at night (Fry et al., 2013). Thus we might expect to see different OA production in nighttime vs. daytime. Figure 7 shows daytime and nighttime OA enhancement as a function of eq. age and OH_{exp} . During all times of the day, OA enhancement was largest in the range of 0.4–1.5 eq. days of photochemical aging, hereafter referred to as the age range of maximum OA enhancement. The diurnal profile of the OA enhancement in this range (inset of Fig. 7) shows that the maximum OA enhancement follows

In situ secondary organic aerosol formation from ambient pine forest air

B. B. Palm et al.

[Title Page](#)

[Abstract](#)

[Introduction](#)

[Conclusions](#)

[References](#)

[Tables](#)

[Figures](#)

[|◀](#)

[▶|](#)

[◀](#)

[▶](#)

[Back](#)

[Close](#)

[Full Screen / Esc](#)

[Printer-friendly Version](#)

[Interactive Discussion](#)



a pattern that is more nuanced than strictly daytime vs. nighttime, with a peak of SOA production in the early morning. Net loss of OA was observed above 10 eq. days of aging, consistent with the LVOC fate model and the interpretation that heterogeneous oxidation dominates at high eq. ages. This is also consistent with previous studies of heterogeneous OH oxidation of OA in a flow tube (George et al., 2008) and with results with the OFR in the Los Angeles urban area (Ortega et al., 2015).

As shown in Fig. 7, OA enhancement shows a strong difference between daytime and nighttime. However, SOA formation potential in the OFR should not be a function of time of day itself. Rather, this is thought to be a coincidental dependence based on the SOA precursor gas concentrations that change in a diurnal manner. In other words, this OH oxidation in the OFR is not reproducing true ambient nighttime chemistry, rather it allows us to measure SOA formation from the true mix of ambient gases during all times of day including nighttime.

These measurements were made in a pine forest dominated by MT (Ortega et al., 2014). As an alternative to separating by time of day, the data are separated by ambient MT concentrations in Fig. 8. The magnitude of SOA formation increased with ambient MT concentrations, ranging from no formation up to greater than $9 \mu\text{g m}^{-3}$ OA enhancement (up to $3 \mu\text{g m}^{-3}$ enhancement without the LVOC fate correction). For the range of ages with maximum OA enhancement (0.4–1.5 eq. days), a correlation is observed between OA enhancement and MT concentrations ($R^2 = 0.47$). Of course, MT may not be the only important precursors driving this correlation. Other gases that are correlated with MT, e.g. sesquiterpenes ($R^2 = 0.70$ with MT shown in Fig. S11) or MT reaction products, may also contribute to the observed correlations. Although MT emissions are strongest during daytime due to their positive temperature dependence, their concentrations are higher at night due to the shallower nighttime boundary layer and reduced oxidation rate (Kim et al., 2010).

We observed much less SOA formation during the daytime, when concentrations of MBO + isoprene peaked but MT concentrations were lower. We note that SOA formation mechanisms that involve heterogeneous uptake followed by multiphase reactions

[Title Page](#)[Abstract](#)[Introduction](#)[Conclusions](#)[References](#)[Tables](#)[Figures](#)[|◀](#)[▶|](#)[◀](#)[▶](#)[Back](#)[Close](#)[Full Screen / Esc](#)[Printer-friendly Version](#)[Interactive Discussion](#)

are not efficiently simulated by the OFR, as their time scales are not shortened proportionally to increased OH concentrations (Hu et al., 2015). This includes the IEPOX pathway from isoprene (Paultot et al., 2009) and the similar pathway proposed for MBO (Zhang et al., 2012), and thus SOA formation potential from MBO + isoprene may be underestimating in our study.

OA enhancement from the OFR185 and OFR254 modes of operation are compared in Fig. 7. Because these were performed with the same physical reactor, we could only perform one of them at a time (see Fig. S7). Since ambient MT concentrations changed over the course of the campaign and they correlated with the amount of SOA formed in the reactor, this effect needed to be corrected before the results of the two reactor modes could be compared. The positive OA enhancement for the OFR254 data was multiplied by the ratio of average MT concentrations between the OFR185 and OFR254 periods (a factor of 1.8). From Fig. 7, we conclude that there were no significant differences in the amount of SOA formation between the OFR185 and OFR254 methods over the range of ages measured in this campaign. Since the OFR185 mode is experimentally simpler and does not require addition of O₃ (with associated issues of mixing, possible contamination, etc.), and since the OFR185 mode more faithfully simulates OH chemistry due to reduced O₃ concentrations (Peng et al., 2015b), we recommend this mode of operation for future OFR studies in forested areas. Additional comparisons of both modes at other locations are also desirable.

3.5 Condensation vs. nucleation in the OFR

When gas-phase molecules are oxidized and achieve a low enough volatility, they can condense onto existing particles (or other surfaces) or nucleate/grow new particles. The difference can be important experimentally because nucleation may produce some particles too small for the size range of the AMS, and it also increases surface area more efficiently than condensation to preexisting particles. Changes in the size distributions measured by the SMPS are used here to investigate the relative importance of these processes.

Particle volume size distributions of air oxidized over the full range of eq. photochemical ages in the flow reactor are shown in Fig. 9, during a period with relatively large OA enhancement in order to clearly demonstrate the behavior. OH oxidation in the reactor resulted in substantial new particle formation and growth, as well as growth of the preexisting ambient particles. The maximum enhancement in both particle modes occurred at an eq. age of ~ 1 day, consistent with AMS measurements of total mass enhancement. At higher ages, the new particle mode decreased in magnitude and diameter and eventually was not present at the highest ages. This is consistent with the results of the LVOC fate model, where at high eq. ages organic gases are rapidly oxidized into smaller volatile products that do not condense. The accumulation mode was also depleted at higher eq. ages, consistent with heterogeneous oxidation leading to fragmentation and evaporation of OA. The observed nucleation at lower eq. ages likely results from some combination of H_2SO_4 and extremely low-volatility organic compounds (ELVOCs; Kirkby et al., 2011; Ehn et al., 2014).

For the data shown in Fig. 9, a larger fraction of SOA molecules condensed onto the freshly nucleated particle mode than onto the preexisting particles. This behavior likely depends on the availability and position of the CS in the size distribution. With the small aerosol concentrations during this campaign, the CS from the new small particles sometimes competed with the CS from ambient particles. During periods when the CS entering the OFR in ambient air was larger, it reduced the condensation of SOA onto new particles, consistent with the lower importance of this mode for an OFR study in the Los Angeles area (Ortega et al., 2015). These results support the possibility of using flow reactors to study the potential for new particle formation and growth in different ambient airmasses and sources (Ezell et al., 2014; Chen et al., 2015).

In situ secondary organic aerosol formation from ambient pine forest air

B. B. Palm et al.

[Title Page](#)

[Abstract](#)

[Introduction](#)

[Conclusions](#)

[References](#)

[Tables](#)

[Figures](#)

[|◀](#)

[▶|](#)

[Back](#)

[Close](#)

[Full Screen / Esc](#)

[Printer-friendly Version](#)

[Interactive Discussion](#)



3.6 Sources of SOA in ambient air

3.6.1 SOA mass formed vs. mass predicted from VOCs

Many previous studies have measured the yields of SOA from oxidation of VOCs in chambers. Those experiments were generally performed under controlled conditions, 5 with detailed information about the type and amount of VOCs available to form SOA at the beginning of the experiment. In this study, we also measured the yield of SOA from oxidation of organic gases, but in this case we started with a complex mixture of ambient organic gases, with some species not being directly measured or speciated. Therefore, the method used here provided a measure of the total SOA formation (or de- 10 struction) as a function of oxidant exposure from *all* ambient gases present, measured and unmeasured. The total SOA formation in the OFR was compared to the amount predicted from measured VOCs. SOA formation was predicted by applying low- NO_x , OA-concentration-dependent, chamber-derived aerosol yields (not including the chemical “aging” parameterization; Tsimpidi et al., 2010) to the percentage of ambient VOC 15 concentrations predicted to react in the OFR based on OH_{exp} ($> 99\%$ of ambient MT, SQT, and isoprene, and $\sim 45\%$ of toluene + *p*-cymene in the age range of 0.4–1.5 eq. days). Previous experiments have shown SOA yields from various precursor gases oxidized in an OFR to be similar to yields from large environmental chambers (Kang et al., 2007, 2011; Lambe et al., 2011b, 2015). With an average post-oxidation OA concentra- 20 tion of $5.1 \mu\text{g m}^{-3}$ with the correction applied, this resulted in campaign-average SOA yields of 13.3, 14.9, 15.9, and 1.8 % for MT, SQT, toluene + *p*-cymene, and isoprene, respectively.

The comparison of maximum measured vs. predicted SOA formation in Fig. 10 shows that approximately 6 times more SOA was formed than predicted from MT, SQT, 25 toluene + *p*-cymene, and isoprene. If the LVOC fate correction is not applied, still 3 times more SOA was measured than predicted (Fig. S12). Note that while the LVOC fate correction led to a factor of ~ 3 increase in OA enhancement (seen in Figs. 7 and 8), it causes only a factor of 2 increase in the slope in Fig. 10. This is because the higher

Title Page

Abstract

Introduction

Conclusions

References

Tables

Figures

|◀

▶|

◀

▶|

Back

Close

Full Screen / Esc

Printer-friendly Version

Interactive Discussion



OA concentrations also lead to higher predicted SOA formation due to increased SOA yields (resulting from increased partitioning to the particle phase).

MT were the dominant SOA precursors, contributing an average of 88 % to predicted SOA formation, with SQT, toluene + *p*-cymene, and isoprene contributing 5, 4, and 5 2 %, respectively. Other known VOCs that form SOA, such as benzene or xylenes, were present in such low concentrations that they would contribute even smaller percentages to predicted SOA formation, so they were not included in this analysis.

The correlation between measured and predicted SOA was $R^2 = 0.58$, indicating that SOA formation potential was controlled mainly by MT and other biogenic gases with 10 similar concentration diurnal patterns, including SQT. Toluene also likely originated at least partially from biogenic sources at this site (Misztal et al., 2015). A diurnal plot of the measured maximum (0.4–1.5 eq. days age) and predicted SOA formation is shown in Fig. 11, along with ambient MT, SQT, toluene +*p*-cymene, and MBO + isoprene concentrations. SOA formation followed a similar diurnal pattern to MT, SQT, and toluene 15 +*p*-cymene, including a substantial increase just after sunrise at 07:00 LT. SOA formation in the OFR followed a very different diurnal pattern than ambient MBO + isoprene, supporting the conclusion that MBO + isoprene was an insignificant contributor to SOA formation in the OFR for the ambient conditions of this campaign.

In order for SOA formation in the OFR to be fully explained by the ambient VOCs, the 20 SOA yields would have needed to be approximately a factor of 6 larger than the values used in this analysis. This would mean, e.g., a 78 % yield from MT with the OA concentrations of only $5.1 \mu\text{g m}^{-3}$ (33 % if the LVOC fate correction is not applied), which is inconsistent with previous OFR and chamber studies that have only achieved such high 25 SOA yields in experiments with over an order of magnitude higher OA concentrations (Kang et al., 2007, 2011; Tsimpidi et al., 2010; Lambe et al., 2011b, 2015). Accounting for S/IVOC wall losses in such experiments (Matsunaga and Ziemann, 2010; Zhang et al., 2014) or including aging parameterizations (e.g., Tsimpidi et al., 2010) might lessen this discrepancy, but is unlikely to be the entire answer. Therefore, this analysis

Title Page

Abstract

Introduction

Conclusions

References

Tables

Figures

|◀

▶|

◀

▶|

Back

Close

Full Screen / Esc

Printer-friendly Version

Interactive Discussion

strongly suggests that there are other gases in ambient air than the VOCs measured by the PTR-TOF-MS that make important contributions to SOA formation.

3.6.2 SOA mass formed vs. predicted from S/IVOCs

While the lowest-volatility organic matter (i.e., OA) is measured by the AMS and the highest-volatility range (VOCs and some IVOCs) is sampled by the PTR-TOF-MS, there is a substantial range of S/IVOCs between them. The gases that enter the OFR as S/IVOCs are the most likely source of SOA formation causing the factor of 6 discrepancy in Sect. 3.6.1. During the BEACHON-RoMBAS campaign, measurements were made using the TD-EIMS instrument to quantify the bulk (volatility-resolved) ambient S/IVOC mass (Hunter et al., 2015). Other techniques at the site identified and quantified various subsets of the S/IVOCs (Yatavelli et al., 2014; Chan et al., 2015). All of the measurements are compiled in Hunter et al. (2015) to determine the total average organic volatility distribution during the campaign, which shows that S/IVOCs were the only pool of gas-phase species that could possibly produce as much SOA mass as observed in our study. Thus we estimate the in situ SOA yield of S/IVOCs needed to explain SOA formation in the OFR.

The average bulk S/IVOC mass concentrations measured with the TD-EIMS are shown as a function of $\log(C^*)$ in the inset of Fig. 12. In Hunter et al. (2015), this mass was interpreted as being an approximate lower limit to S/IVOC mass, assuming the S/IVOCs measured by Yatavelli et al. (2014), Chan et al. (2015), and by the PTR-TOF-MS were subsets of the TD-EIMS measurement. The upper limit is to assume that each instrument measured a different set of S/IVOCs with no overlap, and would be ~ 3.2 times larger than the mass shown in the inset of Fig. 12. With the substantial temporal overlap between OFR operation and TD-EIMS measurements, it is feasible here to determine the SOA yield of S/IVOCs assuming the lower limit case using the full time series, rather than the average concentrations. However, the overlap between OFR operation and all of the measurements of S/IVOCs included in the upper limit case was not sufficient to allow a full time series analysis. Therefore, we use the campaign-

[Title Page](#)

[Abstract](#)

[Introduction](#)

[Conclusions](#)

[References](#)

[Tables](#)

[Figures](#)

◀

▶

[Back](#)

[Close](#)

[Full Screen / Esc](#)

[Printer-friendly Version](#)

[Interactive Discussion](#)

average ratio of upper limit to lower limit S/IVOC mass (10 vs. $3.1 \mu\text{g m}^{-3}$) to estimate the SOA yield from S/IVOCs for the upper limit case.

Ideally, the total mass of S/IVOCs that would be converted into SOA by oxidation of these gases would be determined by multiplying the mass in each volatility bin by the SOA yields of each bin. Since experimental measurements of the aerosol yields of such gases are generally not available and the ambient mixture of S/IVOCs was not fully speciated, we instead proceed under the assumption that all of the SOA formation that was not due to the previously discussed PTR-TOF-MS-measured VOCs came instead from the mass measured in the $C^* = 10^1\text{--}10^7 \mu\text{g m}^{-3}$ volatility bins. Since SQT are typically in the $C^* = 10^5 \mu\text{g m}^{-3}$ range, we subtracted the SQT mass measured by the PTR-TOF-MS from the bulk S/IVOC mass (a subtraction of 6 % of the total TD-EIMS measurement), to avoid double-counting due to this expected measurement overlap. While MT are in the $C^* = 10^7 \mu\text{g m}^{-3}$ range, the TD-EIMS instrument experiences a loss of sampling efficiency in that bin and MT are not expected to be measured (Hunter et al., 2015).

As shown in Fig. 12, an average SOA yield of 80 % for the bulk S/IVOC mass was required in order to bring the measured vs. predicted SOA formation into agreement in the lower limit S/IVOC mass case. Using the upper limit, an average SOA yield of 24 % is needed. While measurements of SOA yields for speciated S/IVOCs are limited, especially for the relatively low OA concentrations in this study, previous work suggests that this range of 24–80 % yield is reasonable. A yield of 51 % was measured for *n*-heptadecane ($C^* = 10^4 \mu\text{g m}^{-3}$) with OA = $15.4 \mu\text{g m}^{-3}$ under high- NO_x conditions (Presto et al., 2010). Yields can be even higher from cyclic compounds (Lim and Ziemann, 2009; Tkacik et al., 2012), and under low- NO_x conditions (Ng et al., 2007; Lane et al., 2008). SOA yields from several other IVOCs (naphthalene and alkyl naphthalenes) under low- NO_x conditions were determined to be 58–73 % with OA concentrations of $10\text{--}40 \mu\text{g m}^{-3}$ (Chan et al., 2009).

When including SOA produced from S/IVOC oxidation in Fig. 12, the correlation between measured and predicted SOA formation was $R^2 = 0.68$. Attempts were made to

5

10

15

20

25

In situ secondary organic aerosol formation from ambient pine forest air

B. B. Palm et al.

[Title Page](#)

[Abstract](#)

[Introduction](#)

[Conclusions](#)

[References](#)

[Tables](#)

[Figures](#)

[|◀](#)

[▶|](#)

[◀](#)

[▶](#)

[Back](#)

[Close](#)

[Full Screen / Esc](#)

[Printer-friendly Version](#)

[Interactive Discussion](#)



optimize the correlation between measured and predicted SOA formation by applying C^* -dependent yields, but this did not result in significantly better correlations. Since speciated S/IVOC measurements as well as yields for each volatility bin (which may have varied with diurnal changes in the composition of each bin) were not available, we concluded that further detailed interpretation of SOA production from the measured S/IVOCs would be under-constrained.

This analysis suggests that OH oxidation of organic gases in a parcel of ambient pine forest air will produce approximately 5 times more SOA from S/IVOC gases than from VOCs. This does not provide information about the sources of the lower volatility organic gases in this parcel. They may be directly emitted, formed as oxidation products of VOCs that were emitted upwind of this parcel, or some combination of these two options. The high correlation between SOA formation and ambient MT concentrations suggests that the S/IVOCs likely came from a biogenic source related to the emission of MT. At night, O_3 and NO_3 may react with the C=C-containing MT and SQT emissions leading to a buildup of S/IVOC oxidation products that lack C=C double bonds, molecules with which O_3 and NO_3 generally do not react (Atkinson, 1997). Variations in the ratio of measured to predicted SOA formation in Figs. 10 and 12 could be due partly to variations in the ratio of the concentrations of S/IVOCs to VOCs due to changes in the meteorological or chemical conditions of the atmosphere, or from periodic changes in the biogenic and/or anthropogenic sources of S/IVOCs.

3.6.3 Sensitivity to LVOC fate model parameters

The LVOC fate correction in this analysis led to a relatively large factor of 3 increase in OA enhancement and factor of 2 increase in measured vs. predicted SOA formation. As the values of several of the model parameters are not well constrained, in this section we investigate the sensitivity of the LVOC fate correction to these parameters. Figure 13 shows the sensitivity of the slope of measured vs. predicted SOA formation from VOCs, as well as how that affected the range of SOA yields needed from S/IVOCs in order to explain the total SOA formation in the OFR. Sensitivity was tested for k_{OH} ,

[Title Page](#)[Abstract](#)[Introduction](#)[Conclusions](#)[References](#)[Tables](#)[Figures](#)[|◀](#)[▶|](#)[◀](#)[▶](#)[Back](#)[Close](#)[Full Screen / Esc](#)[Printer-friendly Version](#)[Interactive Discussion](#)

the number of reactions with OH before LVOCs are lost to volatile, non-condensable products, the SMPS size distribution used to calculate CS, α , k_e , and D .

The least-well-defined parameters in the model were likely k_{OH} and the number of reactions with OH, especially since the analysis of H_2SO_4 condensation in Sect. 3.3.2 did not use them. However, the LVOC fate correction was relatively insensitive to these parameters, specifically for values of k_{OH} less than $3 \times 10^{-11} \text{ cm}^3 \text{ molec}^{-1} \text{ s}^{-1}$ or when assuming 2+ reactions with OH. If we assume LVOCs always remain available to condense and never fragment, the slope reaches a lower asymptote of 5.6. The model also showed a relatively low sensitivity to k_e and D over several orders of magnitude.

The slope of measured vs. predicted SOA formation was more sensitive to the choice of CS and α . The slope is mainly sensitive to CS when approaching the ambient (smaller) value. Since using the average value of CS worked well for the H_2SO_4 analysis (and the ambient CS gave poor results there), it is likely that the average CS is at least close enough to the proper value as not to cause systematic biases. Using values of α less than 1 led to a rapid increase in the magnitude of the LVOC fate correction. Values less than approximately $\alpha = 0.3$ would require the SOA yield from S/IVOCs to approach 100 % as a lower limit, which is unlikely to be the case. In other words, if the sticking coefficient was very low (e.g. $\alpha < 0.1$) it would be impossible to explain the amount of SOA formed from the carbon present in the gas-phase. This suggests that $\alpha = 1$ or close to 1 is a good approximation for the conditions in the OFR at this campaign, and allows us to rule out values much lower than 1.

It is noteworthy that none of the changes to these four parameters led to a substantial decrease in the slope of measured vs. predicted SOA formation. The parameters that can lead to a considerable increase in F_{aer} are the CS and residence time of the OFR (i.e., time allowed for condensation onto particles, which is controlled by flow rate). However, these values were among the best constrained parameters, since we had direct measurements of both during the campaign. This suggests that while the LVOC fate correction was relatively large, it was unlikely to be much smaller.

Title Page	
Abstract	Introduction
Conclusions	References
Tables	Figures
◀	▶
◀	▶
Back	Close
Full Screen / Esc	
Printer-friendly Version	
Interactive Discussion	

4 Conclusions

During the BEACHON-RoMBAS campaign, ambient air was oxidized by OH in an OFR to study in situ SOA formation from the ambient mixture of SOA precursors as they exist in a forest environment. SOA formation was measured semi-continuously, 5 and the changes in both gas and particle phases were documented as a function of photochemical age. The amount of SOA formation increased with age to a maximum at 0.4–1.5 days of eq. photochemical aging, coinciding with depletion of known SOA precursors measured with the PTR-TOF-MS. SOA formation in the OFR correlated with MT concentrations, both of which were typically larger during nighttime. The Net 10 SOA loss was observed at > 10 days eq. age, consistent with heterogeneous oxidation processes being important only for the longest lived aerosol (e.g., free tropospheric aerosol). Similar amounts of SOA formation were observed from both the OFR185 and OFR254 methods over the range of eq. ages used during this campaign. Condensation onto preexisting ambient particles and nucleation and growth of small particles were 15 both observed.

A modeling analysis of the fate of LVOCs in the OFR was presented. The validity of this model was evaluated using the simpler process of SO_2 gas conversion to SO_4 aerosol. The fraction of LVOCs that condense onto aerosols, vs. the other fates of LVOCs including condensing on the reactor walls, exiting the reactor to condense 20 on sampling lines, or reacting with OH to produce volatile fragmentation products, depends strongly on the aerosol surface area available for condensation. Our measurements rule out sticking coefficients much lower than 1. For ambient experiments in rural areas with low CS, laboratory experiments without seed aerosol, or when sampling with a relatively short residence time, a large correction may be required. Addition 25 of an aerosol seed to sample air with low aerosol CS (such as this study) would reduce the uncertainties associated with the LVOC fate correction. In urban areas or in laboratory studies with large seed aerosol surface area, the correction can be much smaller (< 20 %). In either case, the relative time scales of key processes in the OFR need

[Title Page](#)[Abstract](#)[Introduction](#)[Conclusions](#)[References](#)[Tables](#)[Figures](#)[|◀](#)[▶|](#)[Back](#)[Close](#)[Full Screen / Esc](#)[Printer-friendly Version](#)[Interactive Discussion](#)

In situ secondary organic aerosol formation from ambient pine forest air

B. B. Palm et al.

[Title Page](#)[Abstract](#)[Introduction](#)[Conclusions](#)[References](#)[Tables](#)[Figures](#)[|◀](#)[▶|](#)[◀](#)[▶](#)[Back](#)[Close](#)[Full Screen / Esc](#)[Printer-friendly Version](#)[Interactive Discussion](#)

to be carefully considered in order to properly interpret the results of measured SOA formation.

The amount of SOA that could be produced from OH oxidation of the major VOC species measured at this site (MT, SQT, toluene + *p*-cymene, and isoprene) was insufficient to explain the measured SOA formation in the reactor by a factor of 6. A discrepancy this large is unlikely to be explained by incorrect yields for the speciated VOCs or by experimental uncertainties. The correlation between measured and predicted SOA formation suggests that the unidentified SOA precursors were of biogenic origin with a similar diurnal pattern to MT, SQT, and toluene + *p*-cymene. Novel TD-EIMS measurements quantified the reservoir of S/IVOCs, which are not measured efficiently by a PTR-TOF-MS and represent the only pool of gas-phase carbon at the site that could possibly explain the observed SOA. An SOA yield of 24–80 % for the total mass of S/IVOCs measured was required to account for all of the SOA formation from OH oxidation in the OFR. This research points to a need to improve our understanding and measurement capabilities of S/IVOCs.

We have demonstrated how an OFR can be used in combination with a variety of aerosol and gas instruments to provide information about the net SOA formation potential of forest air. The OFR technique allows investigating the quantity and variability of SOA precursor gases that are present in ambient air. These results could be used to inform the treatment of S/IVOCs, such as VOC oxidation products, in SOA models. Future OFR experiments could be designed with additional specialized instrumentation to determine the molecular identities of S/IVOCs and investigate their specific SOA yields.

**The Supplement related to this article is available online at
doi:10.5194/acpd-15-30409-2015-supplement.**

Acknowledgements. We thank US NSF grants AGS-1243354 and AGS-1360834, NOAA grants NA13OAR4310063 and NA10OAR4310106, U.S. DOE ASR Program (Office of Science, BER, DE-SC0011105), Austrian Science Fund (FWF) project number L518-N20, and the US EPA

(STAR 83587701-0) for partial support for this research. B. B. Palm acknowledges support from a CIRES Graduate Student Research Fellowship and a US EPA STAR Graduate Fellowship (FP-91761701-0). L. Kaser acknowledges support from DOC-fFORTE-fellowship of the Austrian Academy of Science. This work has not been formally reviewed by the US EPA. The views expressed are solely those of the authors, and the US EPA does not endorse any products or commercial services mentioned in this work. A. M. Ortega acknowledges a fellowship from the DOE SCGP Fellowship Program (ORAU, ORISE). We are grateful to Alex Guenther and Jim Smith of NCAR for co-organizing the BEACHON-RoMBAS field campaign, to Andrew Turnipseed for SO₂ measurements, and to the USFS Manitou Experimental Forest Observatory for site support.

References

- Alarcón, P., Bohn, B., Zetzsch, C., Rayez, M.-T., and Rayez, J.-C.: Reversible addition of the OH radical to *p*-cymene in the gas phase: multiple adduct formation. Part 2., Phys. Chem. Chem. Phys., 16, 17315–17326, 2014.
- Atkinson, R.: Gas-phase tropospheric chemistry of volatile organic compounds: 1. alkanes and alkenes, J. Phys. Chem. Ref. Data, 26, 215, doi:10.1063/1.556012, 1997.
- Atkinson, R. and Arey, J.: Gas-phase tropospheric chemistry of biogenic volatile organic compounds: a review, Atmos. Environ., 37, 197–219, doi:10.1016/S1352-2310(03)00391-1, 2003.
- Bruns, E. A., El Haddad, I., Keller, A., Klein, F., Kumar, N. K., Pieber, S. M., Corbin, J. C., Slowik, J. G., Brune, W. H., Baltensperger, U., and Prévôt, A. S. H.: Inter-comparison of laboratory smog chamber and flow reactor systems on organic aerosol yield and composition, Atmos. Meas. Tech., 8, 2315–2332, doi:10.5194/amt-8-2315-2015, 2015.
- Calvert, J. G., Atkinson, R., Becker, K. H., Kamens, R. M., Seinfeld, J. H., Wallington, T. H., and Yarwood, G.: The Mechanisms of Atmospheric Oxidation of the Aromatic Hydrocarbons, Oxford University Press, New York, USA, 2002.
- Cappa, C. D. and Jimenez, J. L.: Quantitative estimates of the volatility of ambient organic aerosol, Atmos. Chem. Phys., 10, 5409–5424, doi:10.5194/acp-10-5409-2010, 2010.
- Chan, A. W. H., Kautzman, K. E., Chhabra, P. S., Surratt, J. D., Chan, M. N., Crounse, J. D., Kürten, A., Wennberg, P. O., Flagan, R. C., and Seinfeld, J. H.: Secondary organic aerosol

Title Page

Abstract

Introduction

Conclusions

References

Tables

Figures

◀

▶

◀

▶

Back

Close

Full Screen / Esc

Printer-friendly Version

Interactive Discussion



In situ secondary organic aerosol formation from ambient pine forest air

B. B. Palm et al.

formation from photooxidation of naphthalene and alkyl naphthalenes: implications for oxidation of intermediate volatility organic compounds (IVOCs), *Atmos. Chem. Phys.*, 9, 3049–3060, doi:10.5194/acp-9-3049-2009, 2009.

Chan, A. W. H., Kreisberg, N. M., Hohaus, T., Campuzano-Jost, P., Zhao, Y., Day, D. A., Kaser, L., Karl, T., Hansel, A., Teng, A. P., Ruehl, C. R., Sueper, D. T., Jayne, J. T., Worsnop, D. R., Jimenez, J. L., Hering, S. V., and Goldstein, A. H.: Speciated measurements of semivolatile and intermediate volatility organic compounds (S/IVOCs) in a pine forest during BEACHON-RoMBAS 2011, *Atmos. Chem. Phys. Discuss.*, 15, 22331–22377, doi:10.5194/acpd-15-22331-2015, 2015.

Chen, H., Ezell, M. J., Arquero, K. D., Varner, M. E., Dawson, M. L., Gerber, R. B., and Finlayson-Pitts, B. J.: New particle formation and growth from methanesulfonic acid, trimethylamine and water, *Phys. Chem. Chem. Phys.*, 17, 13699–13709, doi:10.1039/C5CP00838G, 2015.

Cross, E. S., Hunter, J. F., Carrasquillo, A. J., Franklin, J. P., Herndon, S. C., Jayne, J. T., Worsnop, D. R., Miake-Lye, R. C., and Kroll, J. H.: Online measurements of the emissions of intermediate-volatility and semi-volatile organic compounds from aircraft, *Atmos. Chem. Phys.*, 13, 7845–7858, doi:10.5194/acp-13-7845-2013, 2013.

DeCarlo, P. F., Kimmel, J. R., Trimborn, A., Northway, M. J., Jayne, J. T., Aiken, A. C., Gonin, M., Fuhrer, K., Horvath, T., Docherty, K. S., Worsnop, D. R., and Jimenez, J. L.: Field-deployable, high-resolution, time-of-flight aerosol mass spectrometer, *Anal. Chem.*, 78, 8281–8289, doi:10.1021/ac061249n, 2006.

DeCarlo, P. F., Dunlea, E. J., Kimmel, J. R., Aiken, A. C., Sueper, D., Crounse, J., Wennberg, P. O., Emmons, L., Shinozuka, Y., Clarke, A., Zhou, J., Tomlinson, J., Collins, D. R., Knapp, D., Weinheimer, A. J., Montzka, D. D., Campos, T., and Jimenez, J. L.: Fast airborne aerosol size and chemistry measurements above Mexico City and Central Mexico during the MILAGRO campaign, *Atmos. Chem. Phys.*, 8, 4027–4048, doi:10.5194/acp-8-4027-2008, 2008.

Donahue, N. M., Robinson, A. L., Stanier, C. O., and Pandis, S. N.: Coupled partitioning, dilution, and chemical aging of semivolatile organics, *Environ. Sci. Technol.*, 40, 2635–2643, doi:10.1021/es052297c, 2006.

Ehn, M., Thornton, J. A., Kleist, E., Sipilä, M., Junninen, H., Pullinen, I., Springer, M., Rubach, F., Tillmann, R., Lee, B., Lopez-Hilfiker, F., Andres, S., Acir, I.-H., Rissanen, M., Jokinen, T., Schobesberger, S., Kangasluoma, J., Kontkanen, J., Nieminen, T., Kurtén, T.,

[Title Page](#)

[Abstract](#)

[Introduction](#)

[Conclusions](#)

[References](#)

[Tables](#)

[Figures](#)

[|◀](#)

[▶|](#)

[◀](#)

[▶](#)

[Back](#)

[Close](#)

[Full Screen / Esc](#)

[Printer-friendly Version](#)

[Interactive Discussion](#)



- Nielsen, L. B., Jørgensen, S., Kjaergaard, H. G., Canagaratna, M., Maso, M. D., Berndt, T., Petäjä, T., Wahner, A., Kerminen, V.-M., Kulmala, M., Worsnop, D. R., Wildt, J., and Mentel, T. F.: A large source of low-volatility secondary organic aerosol, *Nature*, 506, 476–479, doi:10.1038/nature13032, 2014.
- 5 Ervens, B.: Modeling the processing of aerosol and trace gases in clouds and fogs, *Chem. Rev.*, 115, 4157–4198, doi:10.1021/cr5005887, 2015.
- Ervens, B., Turpin, B. J., and Weber, R. J.: Secondary organic aerosol formation in cloud droplets and aqueous particles (aqSOA): a review of laboratory, field and model studies, *Atmos. Chem. Phys.*, 11, 11069–11102, doi:10.5194/acp-11-11069-2011, 2011.
- 10 Ezell, M. J., Chen, H., Arquero, K. D., and Finlayson-pitts, B. J.: Aerosol fast flow reactor for laboratory studies of new particle formation, *J. Aerosol Sci.*, 78, 30–40, doi:10.1016/j.jaerosci.2014.08.009, 2014.
- Fry, J. L., Draper, D. C., Zarzana, K. J., Campuzano-Jost, P., Day, D. A., Jimenez, J. L., Brown, S. S., Cohen, R. C., Kaser, L., Hansel, A., Cappellin, L., Karl, T., Hodzic Roux, A., Turnipseed, A., Cantrell, C., Lefer, B. L., and Grossberg, N.: Observations of gas- and aerosol-phase organic nitrates at BEACHON-RoMBAS 2011, *Atmos. Chem. Phys.*, 13, 8585–8605, doi:10.5194/acp-13-8585-2013, 2013.
- 15 George, I. J., Slowik, J., and Abbatt, J. P. D.: Chemical aging of ambient organic aerosol from heterogeneous reaction with hydroxyl radicals, *Geophys. Res. Lett.*, 35, L13811, doi:10.1029/2008GL033884, 2008.
- 20 Goldstein, A. H. and Galbally, I. E.: Known and unexplored organic constituents in the earth's atmosphere, *Environ. Sci. Technol.*, 41, 1514–1521, 2007.
- Grieshop, A. P., Logue, J. M., Donahue, N. M., and Robinson, A. L.: Laboratory investigation of photochemical oxidation of organic aerosol from wood fires 1: measurement and simulation 25 of organic aerosol evolution, *Atmos. Chem. Phys.*, 9, 1263–1277, doi:10.5194/acp-9-1263-2009, 2009.
- Hanson, D. R. and Eisele, F.: Diffusion of H_2SO_4 in humidified nitrogen: hydrated H_2SO_4 , *J. Phys. Chem. A*, 104, 1715–1719, 2000.
- 30 Hayes, P. L., Carlton, A. G., Baker, K. R., Ahmadov, R., Washenfelder, R. A., Alvarez, S., Rappenglück, B., Gilman, J. B., Kuster, W. C., de Gouw, J. A., Zotter, P., Prévôt, A. S. H., Szidat, S., Kleindienst, T. E., Offenberg, J. H., Ma, P. K., and Jimenez, J. L.: Modeling the formation and aging of secondary organic aerosols in Los Angeles during CalNex 2010, *Atmos. Chem. Phys.*, 15, 5773–5801, doi:10.5194/acp-15-5773-2015, 2015.

In situ secondary organic aerosol formation from ambient pine forest air

B. B. Palm et al.

[Title Page](#)

[Abstract](#)

[Introduction](#)

[Conclusions](#)

[References](#)

[Tables](#)

[Figures](#)

[|◀](#)

[▶|](#)

[◀](#)

[▶](#)

[Back](#)

[Close](#)

[Full Screen / Esc](#)

[Printer-friendly Version](#)

[Interactive Discussion](#)



- Hodzic, A., Jimenez, J. L., Madronich, S., Canagaratna, M. R., DeCarlo, P. F., Kleinman, L., and Fast, J.: Modeling organic aerosols in a megacity: potential contribution of semi-volatile and intermediate volatility primary organic compounds to secondary organic aerosol formation, *Atmos. Chem. Phys.*, 10, 5491–5514, doi:10.5194/acp-10-5491-2010, 2010.
- Hu, W., Palm, B. B., Day, D. A., Campuzano-Jost, P., Krechmer, J. E., de Sá, S. S., Martin, S. T., Alexander, M. L., Canonaco, F., Prevot, A. S. H., Brune, W. H., and Jimenez, J.-L.: Aging and low volatility of ambient isoprene epoxydiols-derived secondary organic aerosol (IEPOX-SOA): determination of hydroxyl radical (OH) reactive uptake coefficient (γ), in prep., 2015.
- Huffman, J. A., Ziemann, P. J., Jayne, J. T., Worsnop, D. R., and Jimenez, J. L.: Development and characterization of a fast-stepping/scanning thermodenuder for chemically-resolved aerosol volatility measurements, *Aerosol Sci. Tech.*, 42, 395–407, doi:10.1080/02786820802104981, 2008.
- Hunter, J. F., Day, D. A., Yatavelli, R. L. N., Chan, A. W. H., Kaser, L., Cappellin, L., Hayes, P. L., Palm, B. B., Cross, E. S., Carrasquillo, A. J., Campuzano-Jost, P., Stark, H., Zhao, Y., Hohaus, T., Smith, J. N., Hansel, A., Karl, T., Goldstein, A. H., Guenther, A., Worsnop, D., Thornton, J. A., Heald, C. L., Jimenez, J. L., and Kroll, J. H.: Comprehensive characterization of atmospheric organic carbon at a forested site, *Nat. Geosci.*, in revision, 2015.
- IPCC: IPCC 2013: Climate Change 2013: the Physical Science Basis. Contribution of Working Group I to the Fifth Assessment Report of the Intergovernmental Panel on Climate Change, edited by: Stocker, T. F., Qin, D., Plattner, G., Tignor, M., Allen, S. K., Bex, V., and Midgley, P. M., Cambridge University Press, Cambridge, UK, New York, NY, USA, 2013.
- Jimenez, J. L., Canagaratna, M. R., Donahue, N. M., Prevot, A. S. H., Zhang, Q., Kroll, J. H., DeCarlo, P. F., Allan, J. D., Coe, H., Ng, N. L., Aiken, A. C., Docherty, K. S., Ulbrich, I. M., Grieshop, A. P., Robinson, A. L., Duplissy, J., Smith, J. D., Wilson, K. R., Lanz, V. A., Hueglin, C., Sun, Y. L., Tian, J., Laaksonen, A., Raatikainen, T., Rautiainen, J., Vaattovaara, P., Ehn, M., Kulmala, M., Tomlinson, J. M., Collins, D. R., Cubison, M. J., Dunlea, J., Huffman, J. A., Onasch, T. B., Alfarra, M. R., Williams, P. I., Bower, K., Kondo, Y., Schneider, J., Drewnick, F., Borrmann, S., Weimer, S., Demerjian, K., Salcedo, D., Cottrell, L., Griffin, R., Takami, A., Miyoshi, T., Hatakeyama, S., Shimono, A., Sun, J. Y., Zhang, Y. M., Dzepina, K., Kimmel, J. R., Sueper, D., Jayne, J. T., Herndon, S. C., Trimborn, A. M., Williams, L. R., Wood, E. C., Middlebrook, A. M., Kolb, C. E., Baltensperger, U., Worsnop, D. R., Dunlea, E. J., Huffman, J. A., Onasch, T. B., Alfarra, M. R., Williams, P. I., Bower, K., Kondo, Y., Schneider, J., Drewnick, F., Borrmann, S., Weimer, S., Demerjian, K.,

In situ secondary organic aerosol formation from ambient pine forest air

B. B. Palm et al.

[Title Page](#)

[Abstract](#)

[Introduction](#)

[Conclusions](#)

[References](#)

[Tables](#)

[Figures](#)

[|◀](#)

[▶|](#)

[◀](#)

[▶](#)

[Back](#)

[Close](#)

[Full Screen / Esc](#)

[Printer-friendly Version](#)

[Interactive Discussion](#)



- Salcedo, D., Cottrell, L., Griffin, R., Takami, A., Miyoshi, T., Hatakeyama, S., Shimono, A., Sun, J. Y., Zhang, Y. M., Dzepina, K., Kimmel, J. R., Sueper, D., Jayne, J. T., Herndon, S. C., Trimborn, A. M., Williams, L. R., Wood, E. C., Middlebrook, A. M., Kolb, C. E., Baltensperger, U., and Worsnop, D. R.: Evolution of organic aerosols in the atmosphere, *Science*, 326, 1525–1529, doi:10.1126/science.1180353, 2009.
- Julin, J., Winkler, P. M. P., Donahue, N. M., Wagner, P. E., and Riipinen, I.: Near-unity mass accommodation coefficient of organic molecules of varying structure, *Environ. Sci. Technol.*, 48, 12083–12089, doi:10.1021/es501816h, 2014.
- Kang, E., Root, M. J., Toohey, D. W., and Brune, W. H.: Introducing the concept of Potential Aerosol Mass (PAM), *Atmos. Chem. Phys.*, 7, 5727–5744, doi:10.5194/acp-7-5727-2007, 2007.
- Kang, E., Toohey, D. W., and Brune, W. H.: Dependence of SOA oxidation on organic aerosol mass concentration and OH exposure: experimental PAM chamber studies, *Atmos. Chem. Phys.*, 11, 1837–1852, doi:10.5194/acp-11-1837-2011, 2011.
- Karl, T., Hansel, A., Cappellin, L., Kaser, L., Herdlinger-Blatt, I., and Jud, W.: Selective measurements of isoprene and 2-methyl-3-butene-2-ol based on NO⁺ ionization mass spectrometry, *Atmos. Chem. Phys.*, 12, 11877–11884, doi:10.5194/acp-12-11877-2012, 2012.
- Kaser, L., Karl, T., Guenther, A., Graus, M., Schnitzhofer, R., Turnipseed, A., Fischer, L., Harley, P., Madronich, M., Gochis, D., Keutsch, F. N., and Hansel, A.: Undisturbed and disturbed above canopy ponderosa pine emissions: PTR-TOF-MS measurements and MEGAN 2.1 model results, *Atmos. Chem. Phys.*, 13, 11935–11947, doi:10.5194/acp-13-11935-2013, 2013a.
- Kaser, L., Karl, T., Schnitzhofer, R., Graus, M., Herdlinger-Blatt, I. S., DiGangi, J. P., Sive, B., Turnipseed, A., Hornbrook, R. S., Zheng, W., Flocke, F. M., Guenther, A., Keutsch, F. N., Apel, E., and Hansel, A.: Comparison of different real time VOC measurement techniques in a ponderosa pine forest, *Atmos. Chem. Phys.*, 13, 2893–2906, doi:10.5194/acp-13-2893-2013, 2013b.
- Keller, A. and Burtscher, H.: A continuous photo-oxidation flow reactor for a defined measurement of the SOA formation potential of wood burning emissions, *J. Aerosol Sci.*, 49, 9–20, 2012.
- Kim, S., Karl, T., Guenther, A., Tyndall, G., Orlando, J., Harley, P., Rasmussen, R., and Apel, E.: Emissions and ambient distributions of Biogenic Volatile Organic Compounds (BVOC) in a

In situ secondary organic aerosol formation from ambient pine forest air

B. B. Palm et al.

[Title Page](#)

[Abstract](#)

[Introduction](#)

[Conclusions](#)

[References](#)

[Tables](#)

[Figures](#)

[|◀](#)

[▶|](#)

[◀](#)

[▶](#)

[Back](#)

[Close](#)

[Full Screen / Esc](#)

[Printer-friendly Version](#)

[Interactive Discussion](#)



- Kim, S., Wolfe, G. M., Mauldin, L., Cantrell, C., Guenther, A., Karl, T., Turnipseed, A., Greenberg, J., Hall, S. R., Ullmann, K., Apel, E., Hornbrook, R., Kajii, Y., Nakashima, Y., Keutsch, F. N., DiGangi, J. P., Henry, S. B., Kaser, L., Schnitzhofer, R., Graus, M., Hansel, A., Zheng, W., and Flocke, F. F.: Evaluation of HO_x sources and cycling using measurement-constrained model calculations in a 2-methyl-3-butene-2-ol (MBO) and monoterpene (MT) dominated ecosystem, *Atmos. Chem. Phys.*, 13, 2031–2044, doi:10.5194/acp-13-2031-2013, 2013.
- Kirkby, J., Curtius, J., Almeida, J., et al.: Role of sulphuric acid, ammonia and galactic cosmic rays in atmospheric aerosol nucleation, *Nature*, 476, 429–433, doi:10.1038/nature10343, 2011.
- Knote, C., Hodzic, A., and Jimenez, J. L.: The effect of dry and wet deposition of condensable vapors on secondary organic aerosols concentrations over the continental US, *Atmos. Chem. Phys.*, 15, 1–18, doi:10.5194/acp-15-1-2015, 2015.
- Krechmer, J. E., Coggon, M. M., Massoli, P., Nguyen, T. B., Crounse, J. D., Hu, W., Day, D. A., Tyndall, G. S., Henze, D. K., Rivera-Rios, J. C., Nowak, J. B., Kimmel, J. R., Mauldin, R. L., Stark, H., Jayne, J. T., Sipilä, M., Junninen, H., Clair, J. M. St., Zhang, X., Feiner, P. A., Zhang, L., Miller, D. O., Brune, W. H., Keutsch, F. N., Wennberg, P. O., Seinfeld, J. H., Worsnop, D. R., Jimenez, J. L., and Canagaratna, M. R.: Formation of low volatility organic compounds and secondary organic aerosol from isoprene hydroxyhydroperoxide low-NO oxidation, *Environ. Sci. Technol.*, 49, 10330–10339, doi:10.1021/acs.est.5b02031, 2015.
- Kulmala, M. and Wagner, P. E.: Mass accommodation and uptake coefficients – a quantitative comparison, *J. Aerosol Sci.*, 32, 833–841, 2001.
- Lambe, A. T., Ahern, A. T., Williams, L. R., Slowik, J. G., Wong, J. P. S., Abbott, J. P. D., Brune, W. H., Ng, N. L., Wright, J. P., Croasdale, D. R., Worsnop, D. R., Davidovits, P., and Onasch, T. B.: Characterization of aerosol photooxidation flow reactors: heterogeneous oxidation, secondary organic aerosol formation and cloud condensation nuclei activity measurements, *Atmos. Meas. Tech.*, 4, 445–461, doi:10.5194/amt-4-445-2011, 2011a.
- Lambe, A. T., Onasch, T. B., Massoli, P., Croasdale, D. R., Wright, J. P., Ahern, A. T., Williams, L. R., Worsnop, D. R., Brune, W. H., and Davidovits, P.: Laboratory studies of the chemical composition and cloud condensation nuclei (CCN) activity of secondary or-

In situ secondary organic aerosol formation from ambient pine forest air

B. B. Palm et al.

Title Page

Abstract

Introduction

Conclusions

References

Tables

Figures

◀

▶

◀

▶

Back

Close

Full Screen / Esc

Printer-friendly Version

Interactive Discussion



ganic aerosol (SOA) and oxidized primary organic aerosol (OPOA), *Atmos. Chem. Phys.*, 11, 8913–8928, doi:10.5194/acp-11-8913-2011, 2011b.

Lambe, A. T., Chhabra, P. S., Onasch, T. B., Brune, W. H., Hunter, J. F., Kroll, J. H., Cummings, M. J., Brogan, J. F., Parmar, Y., Worsnop, D. R., Kolb, C. E., and Davidovits, P.: Effect of oxidant concentration, exposure time, and seed particles on secondary organic aerosol chemical composition and yield, *Atmos. Chem. Phys.*, 15, 3063–3075, doi:10.5194/acp-15-3063-2015, 2015.

Lane, T. E., Donahue, N. M., and Pandis, S. N.: Effect of NO_x on secondary organic aerosol concentrations, *Environ. Sci. Technol.*, 42, 6022–6027, doi:10.1021/es703225a, 2008.

Lee, A., Goldstein, A. H., Kroll, J. H., Ng, N. L., Varutbangkul, V., Flagan, R. C., and Seinfeld, J. H.: Gas-phase products and secondary aerosol yields from the photooxidation of 16 different terpenes, *J. Geophys. Res.*, 111, D17305, doi:10.1029/2006JD007050, 2006.

Li, R., Palm, B. B., Ortega, A. M., Hlywiak, J., Hu, W., Peng, Z., Day, D. A., Knote, C., Brune, W. H., de Gouw, J. A., and Jimenez, J. L.: Modeling the radical chemistry in an oxidation flow reactor: radical formation and recycling, sensitivities, and the OH exposure estimation equation, *J. Phys. Chem. A*, 119, 4418–4432, 2015.

Lim, Y. B. and Ziemann, P. J.: Effects of molecular structure on aerosol yields from OH radical-initiated reactions of linear, branched, and cyclic alkanes in the presence of NO_x , *Environ. Sci. Technol.*, 43, 2328–2334, doi:10.1021/es803389s, 2009.

Lim, Y. B., Tan, Y., Perri, M. J., Seitzinger, S. P., and Turpin, B. J.: Aqueous chemistry and its role in secondary organic aerosol (SOA) formation, *Atmos. Chem. Phys.*, 10, 10521–10539, doi:10.5194/acp-10-10521-2010, 2010.

Lopez-Hilfiker, F. D., Mohr, C., D'Ambro, E. L., Lutz, A., Irye, S., Riedel, T. P., Surratt, J. D., Lee, B. H., Kurten, T., Hu, W. W., Jimenez, J. L., Carlton, A. G., Baumann, K., Edgerton, E., Hallquist, M., and Thornton, J. A.: Molecular composition and volatility of organic aerosol formed in a polluted isoprene-rich region, *Environ. Sci. Technol.*, under review, 2015.

Mao, J., Ren, X., Brune, W. H., Olson, J. R., Crawford, J. H., Fried, A., Huey, L. G., Cohen, R. C., Heikes, B., Singh, H. B., Blake, D. R., Sachse, G. W., Diskin, G. S., Hall, S. R., and Shetter, R. E.: Airborne measurement of OH reactivity during INTEX-B, *Atmos. Chem. Phys.*, 9, 163–173, doi:10.5194/acp-9-163-2009, 2009.

Matsunaga, A. and Ziemann, P. J.: Gas-wall partitioning of organic compounds in a teflon film chamber and potential effects on reaction product and aerosol yield measurements, *Aerosol Sci. Tech.*, 44, 881–892, doi:10.1080/02786826.2010.501044, 2010.

In situ secondary
organic aerosol
formation from
ambient pine forest
air

B. B. Palm et al.

Title Page

Abstract

Introduction

Conclusions

References

Tables

Figures

◀

▶

Back

Close

Full Screen / Esc

Printer-friendly Version

Interactive Discussion



In situ secondary organic aerosol formation from ambient pine forest air

B. B. Palm et al.

[Title Page](#)

[Abstract](#)

[Introduction](#)

[Conclusions](#)

[References](#)

[Tables](#)

[Figures](#)

[◀](#)

[▶](#)

[◀](#)

[▶](#)

[Back](#)

[Close](#)

[Full Screen / Esc](#)

[Printer-friendly Version](#)

[Interactive Discussion](#)

- McMurtry, P. H. and Grosjean, D.: Gas and aerosol wall losses in Teflon film smog chambers, *Environ. Sci. Technol.*, 19, 1176–1182, doi:10.1021/es00142a006, 1985.
- Miracolo, M. A., Presto, A. A., Lambe, A. T., Hennigan, C. J., Donahue, N. M., Kroll, J. H., Worsnop, D. R., and Robinson, A. L.: Photo-oxidation of low-volatility organics found in motor vehicle emissions: production and chemical evolution of organic aerosol mass, *Environ. Sci. Technol.*, 44, 1638–1643, doi:10.1021/es902635c, 2010.
- Misztal, P. K., Hewitt, C. N., Wildt, J., Blande, J. D., Eller, A. S. D., Fares, S., Gentner, D. R., Gilman, J. B., Graus, M., Greenberg, J., Guenther, A. B., Hansel, A., Harley, P., Huang, M., Jardine, K., Karl, T., Kaser, L., Keutsch, F. N., Kiendler-Scharr, A., Kleist, E., Lerner, B. M., Li, T., Mak, J., Nölscher, A. C., Schnitzhofer, R., Sinha, V., Thornton, B., Warneke, C., Weger, F., Werner, C., Williams, J., Worton, D. R., Yassaa, N., and Goldstein, A. H.: Atmospheric benzenoid emissions from plants rival those from fossil fuels, *Sci. Rep.*, 5, 12064, doi:10.1038/srep12064, 2015.
- Murphy, D. M., Cziczo, D. J., Froyd, K. D., Hudson, P. K., Matthew, B. M., Middlebrook, A. M., Peltier, R. E., Sullivan, A., Thomson, D. S., and Weber, R. J.: Single-particle mass spectrometry of tropospheric aerosol particles, *J. Geophys. Res.*, 111, D23S32, doi:10.1029/2006jd007340, 2006.
- Myhre, G., Shindell, D., Bréon, F.-M., Collins, W., Fuglestvedt, J., Huang, J., Koch, D., Lamarque, J.-F., Lee, D., Mendoza, B., Nakajima, T., Robock, A., Stephens, G., Takemura, T., and Zhang, H.: Anthropogenic and natural radiative forcing, in: Climate Change 2013: the Physical Science Basis. Contribution of Working Group I to the Fifth Assessment Report of the Intergovernmental Panel on Climate Change, edited by: Stocker, T. F., Qin, D., Plattner, G.-K., Tignor, M., Allen, S. K., Boschung, J., Nauels, A., Xia, Y., Bex, V., and Midgley, P. M., Cambridge University Press, Cambridge, UK, New York, NY, USA, 659–740, 2013.
- Ng, N. L., Chhabra, P. S., Chan, A. W. H., Surratt, J. D., Kroll, J. H., Kwan, A. J., McCabe, D. C., Wennberg, P. O., Sorooshian, A., Murphy, S. M., Dalleska, N. F., Flagan, R. C., and Seinfeld, J. H.: Effect of NO_x level on secondary organic aerosol (SOA) formation from the photooxidation of terpenes, *Atmos. Chem. Phys.*, 7, 5159–5174, doi:10.5194/acp-7-5159-2007, 2007.
- Nguyen, T. B., Crounse, J. D., Teng, A. P., St. Clair, J. M., Paulot, F., Wolfe, G. M., and Wennberg, P. O.: Rapid deposition of oxidized biogenic compounds to a temperate forest, *P. Natl. Acad. Sci. USA*, 112, E392–E401, doi:10.1073/pnas.1418702112, 2015.

- Ortega, A. M., Day, D. A., Cubison, M. J., Brune, W. H., Bon, D., de Gouw, J. A., and Jimenez, J. L.: Secondary organic aerosol formation and primary organic aerosol oxidation from biomass-burning smoke in a flow reactor during FLAME-3, *Atmos. Chem. Phys.*, 13, 11551–11571, doi:10.5194/acp-13-11551-2013, 2013.
- 5 Ortega, A. M., Hayes, P. L., Peng, Z., Palm, B. B., Hu, W., Day, D. A., Li, R., Cubison, M. J., Brune, W. H., Graus, M., Warneke, C., Gilman, J. B., Kuster, W. C., de Gouw, J. A., and Jimenez, J. L.: Real-time measurements of secondary organic aerosol formation and aging from ambient air in an oxidation flow reactor in the Los Angeles area, *Atmos. Chem. Phys. Discuss.*, 15, 21907–21958, doi:10.5194/acpd-15-21907-2015, 2015.
- 10 Ortega, J., Turnipseed, A., Guenther, A. B., Karl, T. G., Day, D. A., Gochis, D., Huffman, J. A., Prenni, A. J., Levin, E. J. T., Kreidenweis, S. M., DeMott, P. J., Tobo, Y., Patton, E. G., Hodzic, A., Cui, Y. Y., Harley, P. C., Hornbrook, R. S., Apel, E. C., Monson, R. K., Eller, A. S. D., Greenberg, J. P., Barth, M. C., Campuzano-Jost, P., Palm, B. B., Jimenez, J. L., Aiken, A. C., Dubey, M. K., Geron, C., Offenberg, J., Ryan, M. G., Fornwalt, P. J., Pryor, S. C., Keutsch, F. N., DiGangi, J. P., Chan, A. W. H., Goldstein, A. H., Wolfe, G. M., Kim, S., Kaser, L., Schnitzhofer, R., Hansel, A., Cantrell, C. A., Mauldin, R. L., and Smith, J. N.: Overview of the Manitou Experimental Forest Observatory: site description and selected science results from 2008 to 2013, *Atmos. Chem. Phys.*, 14, 6345–6367, doi:10.5194/acp-14-6345-2014, 2014.
- 15 20 Pankow, J. F.: An absorption model of gas/particle partitioning of organic compounds in the atmosphere, *Atmos. Environ.*, 28, 185–188, doi:10.1016/1352-2310(94)90093-0, 1994.
- 25 Paulot, F., Crounse, J. D., Kjaergaard, H. G., Kürten, A., St Clair, J. M., Seinfeld, J. H., Wennberg, P. O., Kurten, A., St Clair, J. M., Seinfeld, J. H., Wennberg, P. O., Kürten, A., St Clair, J. M., Seinfeld, J. H., and Wennberg, P. O.: Unexpected epoxide formation in the gas-phase photooxidation of isoprene, *Science*, 325, 730–733, doi:10.1126/science.1172910, 2009.
- 30 30 Peng, Z., Day, D. A., Stark, H., Li, R., Palm, B. B., Brune, W. H., and Jimenez, J. L.: HO_x radical chemistry in oxidation flow reactors with low-pressure mercury lamps systematically examined by modeling, *Atmos. Meas. Tech. Discuss.*, 8, 3883–3932, doi:10.5194/amtd-8-3883-2015, 2015a.
- Peng, Z., Day, D. A., Ortega, A. M., Palm, B. B., Hu, W. W., Stark, H., Li, R., Tsigaridis, K., Brune, W. H., and Jimenez, J. L.: Non-OH chemistry in oxidation flow reactors for the study of

In situ secondary organic aerosol formation from ambient pine forest air

B. B. Palm et al.

[Title Page](#)

[Abstract](#)

[Introduction](#)

[Conclusions](#)

[References](#)

[Tables](#)

[Figures](#)

[|◀](#)

[▶|](#)

[◀](#)

[▶](#)

[Back](#)

[Close](#)

[Full Screen / Esc](#)

[Printer-friendly Version](#)

[Interactive Discussion](#)



Pierce, J. R., Engelhart, G. J., Hildebrandt, L., Weitkamp, E. A., Pathak, R. K., Donahue, N. M., Robinson, A. L., Adams, P. J., and Pandis, S. N.: Constraining particle evolution from wall losses, coagulation, and condensation-evaporation in smog-chamber experiments: optimal estimation based on size distribution measurements, *Aerosol Sci. Tech.*, 42, 1001–1015, doi:10.1080/02786820802389251, 2008.

Pirjola, L., Kulmala, M., Wilck, M., Bischoff, A., Stratmann, F., and Otto, E.: Formation of sulphuric acid aerosols and cloud condensation nuclei: an expression for significant nucleation and model comparison, *J. Aerosol Sci.*, 30, 1079–1094, doi:10.1016/S0021-8502(98)00776-9, 1999.

Pope, C. A. and Dockery, D. W.: Health effects of fine particulate air pollution: lines that connect, *J. Air Waste Manage.*, 56, 709–742, doi:10.1080/10473289.2006.10464485, 2006.

Pöschl, U., Canagaratna, M., Jayne, J. T., Molina, L. T., Worsnop, D. R., Kolb, C. E., and Molina, M. J.: Mass accommodation coefficient of H_2SO_4 vapor on aqueous sulfuric acid surfaces and gaseous diffusion coefficient of H_2SO_4 in $\text{N}_2/\text{H}_2\text{O}$, *J. Phys. Chem. A*, 102, 10082–10089, 1998.

Presto, A. A., Miracolo, M. A., Donahue, N. M., and Robinson, A. L.: Secondary organic aerosol formation from high- NO_x photo-oxidation of low volatility precursors: *n*-alkanes, *Environ. Sci. Technol.*, 44, 2029–2034, doi:10.1021/es903712r, 2010.

Robinson, A. L., Donahue, N. M., Shrivastava, M. K., Weitkamp, E. A., Sage, A. M., Grieshop, A. P., Lane, T. E., Pierce, J. R., and Pandis, S. N.: Rethinking organic aerosols: semivolatile emissions and photochemical aging, *Science*, 315, 1259–1262, doi:10.1126/science.1133061, 2007.

Sander, S. P., Friedl, R. R., Barker, J. R., Golden, D. M., Kurylo, M. J., Sciences, G. E., Wine, P. H., Abbatt, J. P. D., Burkholder, J. B., Kolb, C. E., Moortgat, G. K., Huie, R. E., Orkin, V. L., Barker, J. R., Burkholder, J. B., Friedl, R. R., Golden, D. M., Huie, R. E., Kolb, C. E., Kurylo, M. J., Moortgat, G. K., Orkin, V. L., and Wine, P. H.: Chemical Kinetics and Photochemical Data for Use in Atmospheric Studies Evaluation Number 17 NASA Panel for Data Evaluation, JPL Publ. 10-6, Jet Propulsion Laboratory, California Institute of Technology, Pasadena, California, USA, 2011.

Seinfeld, J. H. and Pandis, S. N.: *Atmospheric Chemistry and Physics*, 2nd edn., John Wiley & Sons, Inc., New York, USA, 2006.

In situ secondary organic aerosol formation from ambient pine forest air

B. B. Palm et al.

Title Page

Abstract

Introduction

Conclusions

References

Tables

Figures

◀

▶

◀

▶

Back

Close

Full Screen / Esc

Printer-friendly Version

Interactive Discussion



In situ secondary organic aerosol formation from ambient pine forest air

B. B. Palm et al.

- Smith, J. D., Kroll, J. H., Cappa, C. D., Che, D. L., Liu, C. L., Ahmed, M., Leone, S. R., Worsnop, D. R., and Wilson, K. R.: The heterogeneous reaction of hydroxyl radicals with sub-micron squalane particles: a model system for understanding the oxidative aging of ambient aerosols, *Atmos. Chem. Phys.*, 9, 3209–3222, doi:10.5194/acp-9-3209-2009, 2009.
- Surratt, J. D., Chan, A. W. H., Eddingsaas, N. C., Chan, M., Loza, C. L., Kwan, A. J., Hersey, S. P., Flagan, R. C., Wennberg, P. O., and Seinfeld, J. H.: Reactive intermediates revealed in secondary organic aerosol formation from isoprene., *P. Natl. Acad. Sci. USA*, 107, 6640–6645, doi:10.1073/pnas.0911114107, 2010.
- Tanaka, P. L., Allen, D. T., and Mullins, C. B.: An environmental chamber investigation of chlorine-enhanced ozone formation in Houston, Texas, *J. Geophys. Res.*, 108, 4576, doi:10.1029/2002JD003314, 2003.
- Tang, M. J., Shiraiwa, M., Pöschl, U., Cox, R. A., and Kalberer, M.: Compilation and evaluation of gas phase diffusion coefficients of reactive trace gases in the atmosphere: Volume 2. Diffusivities of organic compounds, pressure-normalised mean free paths, and average Knudsen numbers for gas uptake calculations, *Atmos. Chem. Phys.*, 15, 5585–5598, doi:10.5194/acp-15-5585-2015, 2015.
- Tkacik, D. S., Presto, A. A., Donahue, N. M., and Robinson, A. L.: Secondary organic aerosol formation from intermediate-volatility organic compounds: cyclic, linear, and branched alkanes, *Environ. Sci. Technol.*, 46, 8773–8781, doi:10.1021/es301112c, 2012.
- Tkacik, D. S., Lambe, A. T., Jathar, S., Li, X., Presto, A. A., Zhao, Y., Blake, D., Meinardi, S., Jayne, J. T., Croteau, P. L., and Robinson, A. L.: Secondary organic aerosol formation from in-use motor vehicle emissions using a potential aerosol mass reactor, *Environ. Sci. Technol.*, 48, 11235–11242, doi:10.1021/es502239v, 2014.
- Tsigaridis, K., Daskalakis, N., Kanakidou, M., Adams, P. J., Artaxo, P., Bahadur, R., Balkanski, Y., Bauer, S. E., Bellouin, N., Benedetti, A., Bergman, T., Berntsen, T. K., Beukes, J. P., Bian, H., Carslaw, K. S., Chin, M., Curci, G., Diehl, T., Easter, R. C., Ghan, S. J., Gong, S. L., Hodzic, A., Hoyle, C. R., Iversen, T., Jathar, S., Jimenez, J. L., Kaiser, J. W., Kirkevåg, A., Koch, D., Kokkola, H., Lee, Y. H., Lin, G., Liu, X., Luo, G., Ma, X., Mann, G. W., Mihalopoulos, N., Morcrette, J.-J., Müller, J.-F., Myhre, G., Myrookefalitakis, S., Ng, N. L., O'Donnell, D., Penner, J. E., Pozzoli, L., Pringle, K. J., Russell, L. M., Schulz, M., Sciare, J., Selander, Ø., Shindell, D. T., Sillman, S., Skeie, R. B., Spracklen, D., Stavrakou, T., Steenrod, S. D., Takemura, T., Tiitta, P., Tilmes, S., Tost, H., van Noije, T., van Zyl, P. G., von Salzen, K., Yu, F., Wang, Z., Wang, Z., Zaveri, R. A., Zhang, H., Zhang, K., Zhang, Q., and Zhang, X.: The

[Title Page](#)

[Abstract](#)

[Introduction](#)

[Conclusions](#)

[References](#)

[Tables](#)

[Figures](#)

[|◀](#)

[▶|](#)

[◀](#)

[▶](#)

[Back](#)

[Close](#)

[Full Screen / Esc](#)

[Printer-friendly Version](#)

[Interactive Discussion](#)



Tsimpidi, A. P., Karydis, V. A., Zavala, M., Lei, W., Molina, L., Ulbrich, I. M., Jimenez, J. L., and Pandis, S. N.: Evaluation of the volatility basis-set approach for the simulation of organic aerosol formation in the Mexico City metropolitan area, *Atmos. Chem. Phys.*, 10, 525–546, doi:10.5194/acp-10-525-2010, 2010.

Vaden, T. D., Imre, D., Beranek, J., Shrivastava, M., Zelenyuk, A., Beránek, J., Shrivastava, M., and Zelenyuk, A.: Evaporation kinetics and phase of laboratory and ambient secondary organic aerosol, *P. Natl. Acad. Sci. USA*, 108, 2190–2195, doi:10.1073/pnas.1013391108, 2011.

Volkamer, R., Jimenez, J. L., San Martini, F., Dzepina, K., Zhang, Q., Salcedo, D., Molina, L. T., Worsnop, D. R., and Molina, M. J.: Secondary organic aerosol formation from anthropogenic air pollution: rapid and higher than expected, *Geophys. Res. Lett.*, 33, L17811, doi:10.1029/2006GL026899, 2006.

Wolfe, G. M., Cantrell, C., Kim, S., Mauldin III, R. L., Karl, T., Harley, P., Turnipseed, A., Zheng, W., Flocke, F., Apel, E. C., Hornbrook, R. S., Hall, S. R., Ullmann, K., Henry, S. B., DiGangi, J. P., Boyle, E. S., Kaser, L., Schnitzhofer, R., Hansel, A., Graus, M., Nakashima, Y., Kajii, Y., Guenther, A., and Keutsch, F. N.: Missing peroxy radical sources within a summer-time ponderosa pine forest, *Atmos. Chem. Phys.*, 14, 4715–4732, doi:10.5194/acp-14-4715-2014, 2014.

Yatavelli, R. L. N., Stark, H., Thompson, S. L., Kimmel, J. R., Cubison, M. J., Day, D. A., Campuzano-Jost, P., Palm, B. B., Hodzic, A., Thornton, J. A., Jayne, J. T., Worsnop, D. R., and Jimenez, J. L.: Semicontinuous measurements of gas–particle partitioning of organic acids in a ponderosa pine forest using a MOVI-HRToF-CIMS, *Atmos. Chem. Phys.*, 14, 1527–1546, doi:10.5194/acp-14-1527-2014, 2014.

Zhang, H., Worton, D. R., Lewandowski, M., Ortega, J., Rubitschun, C. L., Park, J.-H., Kristensen, K., Campuzano-Jost, P., Day, D. A., Jimenez, J. L., Jaoui, M., Offenberg, J. H., Klein-dienst, T. E., Gilman, J., Kuster, W. C., de Gouw, J., Park, C., Schade, G. W., Frossard, A. A., Russell, L., Kaser, L., Jud, W., Hansel, A., Cappellin, L., Karl, T., Glasius, M., Guenther, A., Goldstein, A. H., Seinfeld, J. H., Gold, A., Kamens, R. M., and Surratt, J. D.: Organosulfates as tracers for Secondary Organic Aerosol (SOA) formation from 2-Methyl-3-Buten-2-ol (MBO) in the atmosphere, *Environ. Sci. Technol.*, 46, 9437–9446, doi:10.1021/es301648z, 2012.

In situ secondary organic aerosol formation from ambient pine forest air

B. B. Palm et al.

Title Page

Abstract

Introduction

Conclusions

References

Tables

Figures

◀

▶

Back

Close

Full Screen / Esc

Printer-friendly Version

Interactive Discussion



In situ secondary organic aerosol formation from ambient pine forest air

B. B. Palm et al.

[Title Page](#)[Abstract](#)[Introduction](#)[Conclusions](#)[References](#)[Tables](#)[Figures](#)[|◀](#)[▶|](#)[◀](#)[▶](#)[Back](#)[Close](#)[Full Screen / Esc](#)[Printer-friendly Version](#)[Interactive Discussion](#)

Zhang, Q., Jimenez, J. L., Canagaratna, M. R., Allan, J. D., Coe, H., Ulbrich, I., Alfarra, M. R., Takami, A., Middlebrook, A. M., Sun, Y. L., Dzepina, K., Dunlea, E., Docherty, K., DeCarlo, P. F., Salcedo, D., Onasch, T., Jayne, J. T., Miyoshi, T., Shimono, A., Hatakeyama, S., Takegawa, N., Kondo, Y., Schneider, J., Drewnick, F., Borrmann, S., Weimer, S., Demerjian, K., Williams, P., Bower, K., Bahreini, R., Cottrell, L., Griffin, R. J., Rautiainen, J., Sun, J. Y., Zhang, Y. M., and Worsnop, D. R.: Ubiquity and dominance of oxygenated species in organic aerosols in anthropogenically-influenced Northern Hemisphere midlatitudes, *Geophys. Res. Lett.*, 34, L13801, doi:10.1029/2007gl029979, 2007.

Zhang, X., Cappa, C. D., Jathar, S. H., McVay, R. C., Ensberg, J. J., Kleeman, M. J., and Seinfeld, J. H.: Influence of vapor wall loss in laboratory chambers on yields of secondary organic aerosol, *P. Natl. Acad. Sci. USA*, 111, 5802–5807, doi:10.1073/pnas.1404727111, 2014.

Zhao, Y., Hennigan, C. J., May, A. A., Tkacik, D. S., de Gouw, J. A. De, Gilman, J. B., Kuster, W. C., Borbon, A., and Robinson, A. L.: Intermediate-volatility organic compounds: a large source of secondary organic aerosol, *Environ. Sci. Technol.*, 48, 13743–13750, doi:10.1021/es5035188, 2014.

Ziemann, P. J. and Atkinson, R.: Kinetics, products, and mechanisms of secondary organic aerosol formation, *Chem. Soc. Rev.*, 41, 6582–6605, doi:10.1039/c2cs35122f, 2012.

In situ secondary organic aerosol formation from ambient pine forest air

B. B. Palm et al.

[Title Page](#)

[Abstract](#)

[Introduction](#)

[Conclusions](#)

[References](#)

[Tables](#)

[Figures](#)

[|◀](#)

[▶|](#)

[◀](#)

[▶](#)

[Back](#)

[Close](#)

[Full Screen / Esc](#)

[Printer-friendly Version](#)

[Interactive Discussion](#)

Table 1. List of prominent compounds detected by PTR-TOF-MS in the OFR. Likely compound identifications are taken from previous measurements at the same research site, described in Kim et al. (2010) and Kaser et al. (2013a).

Protonated molecular formula	Likely compound(s)	Exact mass (<i>m/z</i>)
$\text{CH}_2\text{O-H}^+$	formaldehyde	31.02
$\text{CH}_4\text{O-H}^+$	methanol	33.03
$\text{C}_2\text{H}_4\text{O-H}^+$	acetaldehyde	45.03
$\text{CH}_2\text{O}_2\text{-H}^+$	formic acid	47.01
$\text{C}_3\text{H}_6\text{O-H}^+$	acetone	59.05
$\text{C}_2\text{H}_4\text{O}_2\text{-H}^+$	acetic acid	61.03
$\text{C}_5\text{H}_8\text{-H}^+$	MBO (~ 80 %) + isoprene (~ 20 %) ^a	69.07
$\text{C}_7\text{H}_8\text{-H}^+$	toluene (74 %) + <i>p</i> -cymene (26 %) ^b	93.07
$\text{C}_{10}\text{H}_{14}\text{-H}^+$	<i>p</i> -cymene	135.12
$\text{C}_{10}\text{H}_{16}\text{-H}^+$	MT	137.13, 81.07
$\text{C}_9\text{H}_{14}\text{O-H}^+$	nopinone	139.11
$\text{C}_{10}\text{H}_{14}\text{O-H}^+$	pinonaldehyde (-H ₂ O), caronaldehyde (-H ₂ O)	151.11
$\text{C}_{10}\text{H}_{16}\text{O-H}^+$	camphor + α -pinene oxide	153.13
$\text{C}_{15}\text{H}_{24}\text{-H}^+$	SQT	205.20

^a Karl et al. (2012); Kaser et al. (2013b).

^b Kaser et al. (2013b).

In situ secondary organic aerosol formation from ambient pine forest air

B. B. Palm et al.

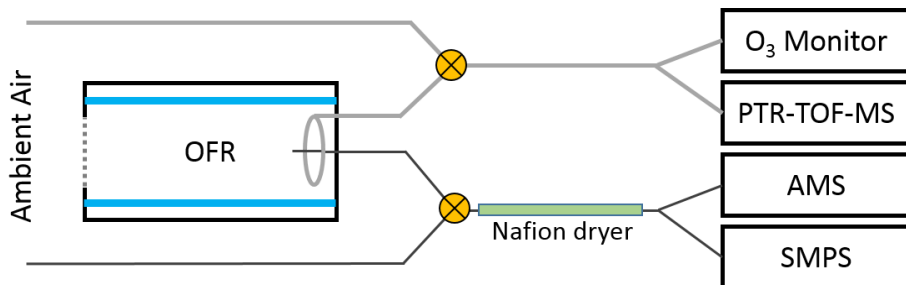


Figure 1. Simplified schematic of the experimental setup. Ambient air was alternately sampled either directly or through the oxidation flow reactor (OFR). In the OFR, the concentration of OH was increased to simulate atmospheric aging from hours up to several weeks.

[Title Page](#)[Abstract](#)[Introduction](#)[Conclusions](#)[References](#)[Tables](#)[Figures](#)[|◀](#)[▶|](#)[◀](#)[▶](#)[Back](#)[Close](#)[Full Screen / Esc](#)[Printer-friendly Version](#)[Interactive Discussion](#)

In situ secondary organic aerosol formation from ambient pine forest air

B. B. Palm et al.

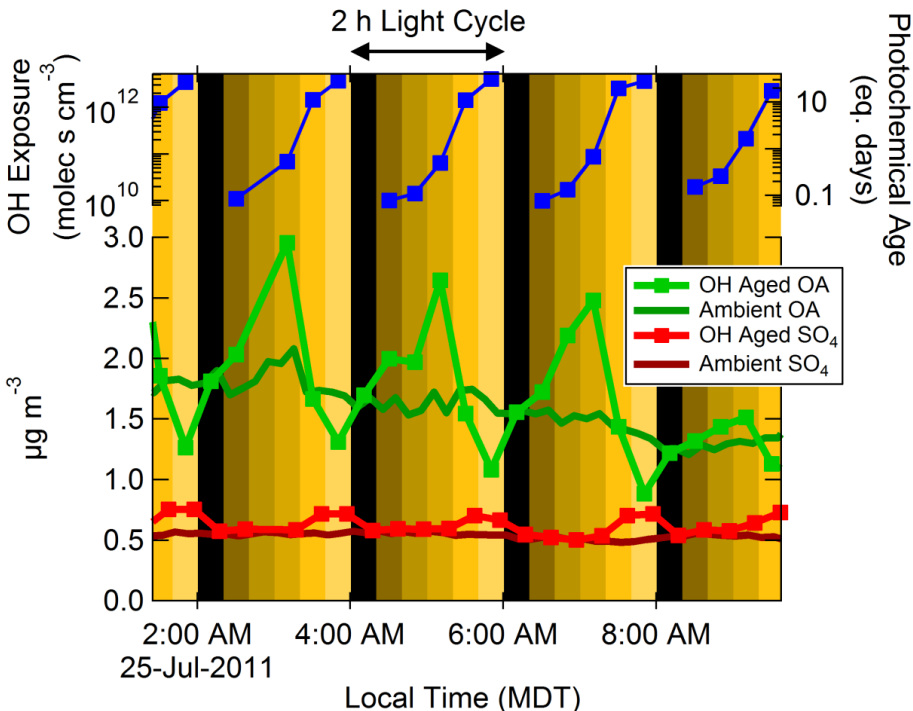


Figure 2. Continuous cycling of OH oxidation using the OFR185 method, compared to concurrent ambient measurements. The sawtooth pattern in the OFR results from OA mass enhancement at low–intermediate OH exposure (OH_{exp}) and decreases at the highest photochemical ages. SO_4 mass increased monotonically with OH_{exp} and at higher exposures, as expected from relatively slow $\text{SO}_2 + \text{OH}$ oxidation and lack of OH destruction of SO_4 .

Title Page

Abstract

Introduction

Conclusion

References

Tables

Figures



Back

Close

Full Screen / Esc

• 10 •

In situ secondary organic aerosol formation from ambient pine forest air

B. B. Palm et al.

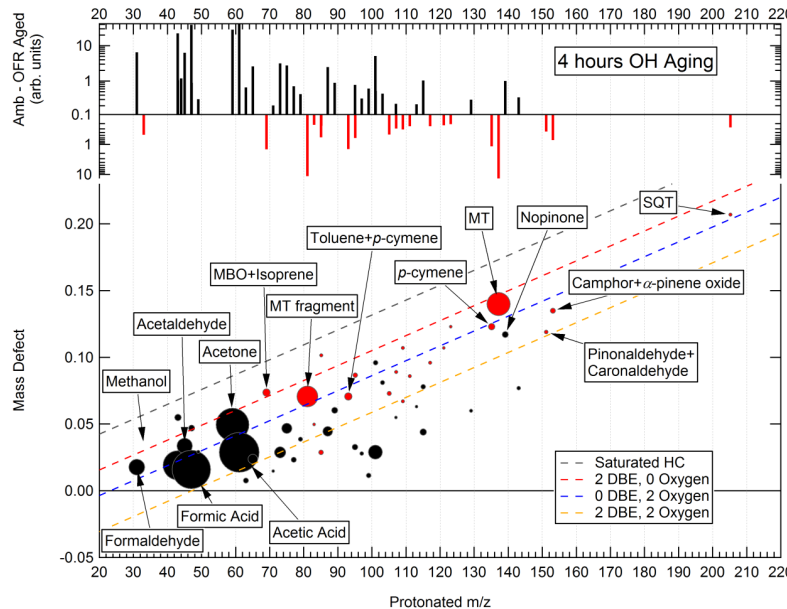


Figure 3. The absolute changes (signal after OH oxidation in the reactor minus ambient signal) of molecules measured by the PTR-TOF-MS after 4 h of eq. aging using the OFR185 method, shown as a difference mass spectrum and in a mass defect diagram. The mass spectra are 10 min averages (5 min from each of the two sample cycles used). The background-subtracted signals are shown in arbitrary units, not corrected for differences in sensitivity of each compound due to the large number of compounds and the inability to positively identify all of them. Prominent molecules are labeled by name or elemental formula assignments. Dashed lines representing molecules with varying double bond equivalents (DBE) or number of oxygen atoms are shown for reference. A red marker signifies that the signal decreased due to oxidation, while a black marker indicates where signal was greater after oxidation. The markers are sized by the square root of the absolute change in signal at each peak after oxidation (i.e., marker area is proportional to signal). Minor signals with absolute change of < 0.2 arb. units or change of < 20 % of total ambient signal were removed.

In situ secondary organic aerosol formation from ambient pine forest air

B. B. Palm et al.

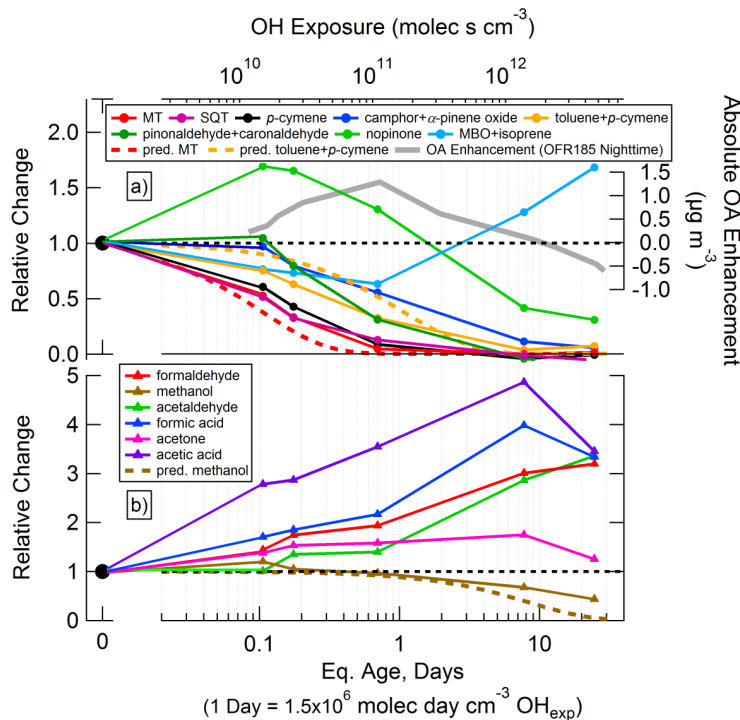


Figure 4. Relative changes in prominent PTR-TOF-MS compounds as a function of photochemical age using the OFR185 method: **(a)** toluene + *p*-cymene and terpene-related signals compared to nighttime OA enhancement using the OFR185 method (not LVOC fate corrected), and **(b)** oxidation products formed in the OFR. For comparison, dashed lines indicate theoretical depletion of an equal mix of α -pinene, β -pinene, and 3-carene (the three major MT at this site; Kim et al., 2010; Ortega et al., 2014), a 74 : 26 mix of toluene + *p*-cymene (Kaser et al., 2013b), and methanol.

Title Page

Abstract

Introduction

Conclusio

References

Tables

Figures



Back

Close

Full Screen / Esc

Interactive Discussion

In situ secondary organic aerosol formation from ambient pine forest air

B. B. Palm et al.

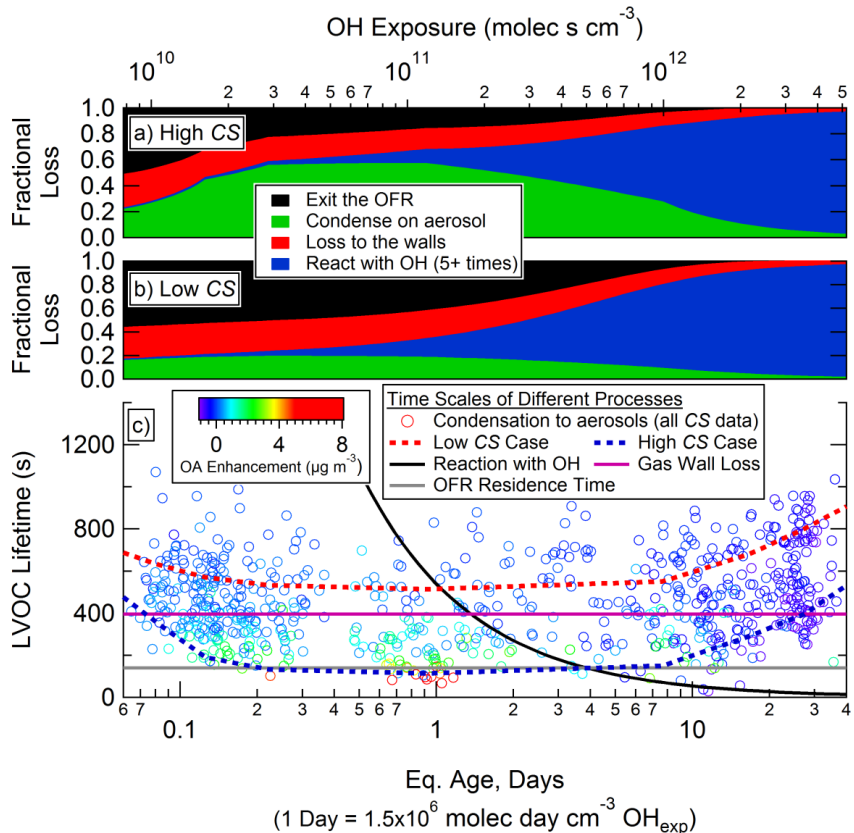


Figure 5. Fractional fates of loss of LVOCs to OFR walls, condensation to aerosols, reaction with OH to produce volatile products, or exiting the OFR to be lost on sampling line walls as a function of photochemical age for **(a)** high CS and **(b)** low CS cases; **(c)** LVOC lifetimes for each of these pathways. Lifetime for condensation to aerosols is shown for all data points (colored by OA enhancement after oxidation) using CS calculated from SMPS measurements.

30463

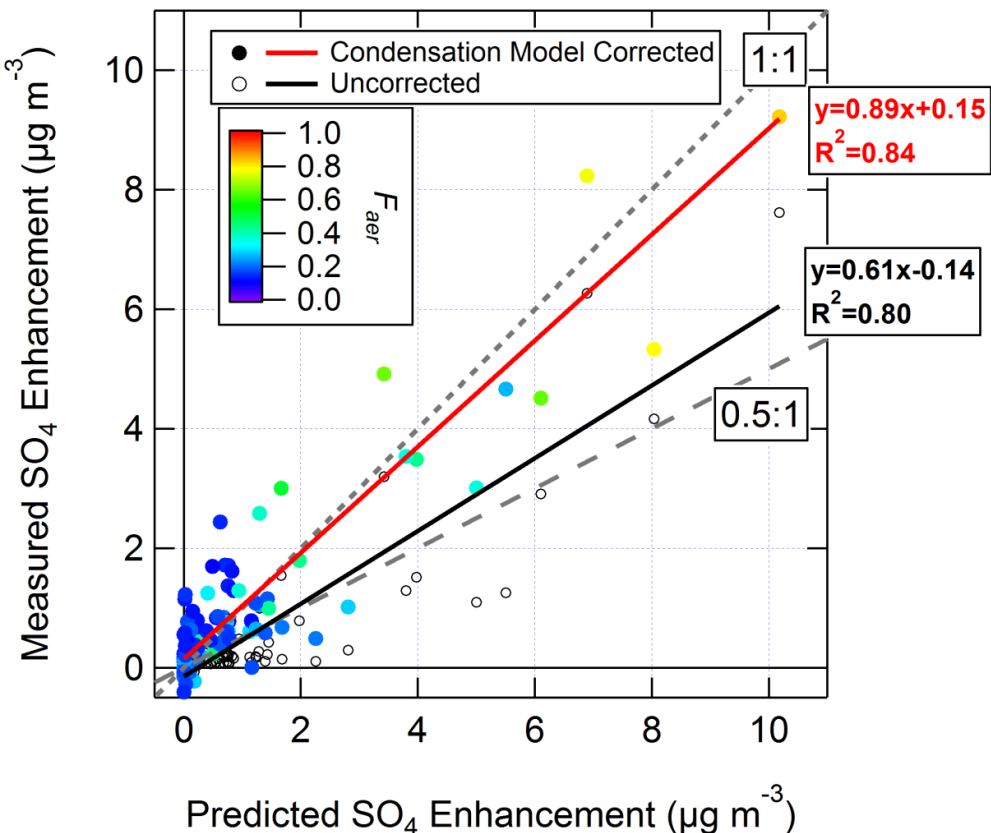


Figure 6. Measured vs. predicted SO_4 formation after OH oxidation in an OFR. The data points are colored by the fraction of H_2SO_4 predicted to condense on aerosols, calculated using $\alpha = 0.65$ and the average of the SMPS size distributions measured before and after oxidation. Data are shown with the LVOC fate correction applied, along with linear fits to the corrected (red) and uncorrected (blue) data.

In situ secondary organic aerosol formation from ambient pine forest air

B. B. Palm et al.

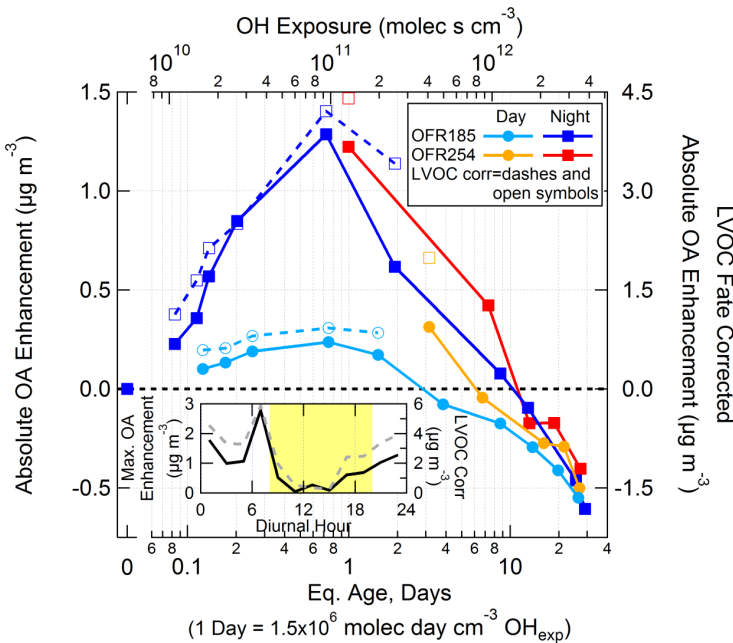


Figure 7. Comparison of absolute OA enhancement from OH oxidation using the OFR185 and OFR254 methods, binned by photochemical age and separated into daytime (08:00–20:00 LT) and nighttime (20:00–08:00 LT) to reflect the changes in ambient SOA precursors between day and night. Data are shown with (right axis, open symbols, and dashed lines) and without (left axis, closed symbols and solid lines) the LVOC fate correction described in Sect. 3.3. Inset: the maximum OA enhancement (all data 0.4–1.5 days eq. age) as a function of time of day, with (dashed) and without (solid) the LVOC fate correction. OFR254 measurements with positive OA enhancement were multiplied by the ratio of ambient MT concentrations measured during OFR185 vs. OFR254 sampling periods (ratio = 1.8). Negative OA enhancements were not normalized in this way since the amount of mass lost due to heterogeneous oxidation would not necessarily correlate with ambient MT concentrations.

In situ secondary organic aerosol formation from ambient pine forest air

B. B. Palm et al.

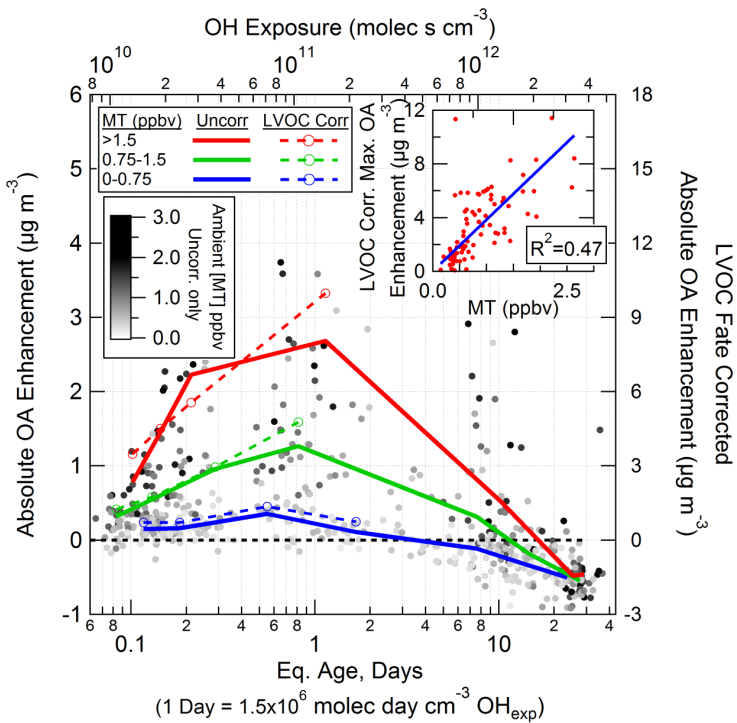


Figure 8. OA enhancement from OH oxidation of ambient air using the OFR185 method as a function of photochemical age. All data points (uncorrected only) are shown, shaded by in-canopy monoterpene (MT) concentrations. Average OA enhancements of age quantiles with equal number of data points with (right axis, dashed lines) and without (left axis, solid lines) the LVOC fate correction are also shown, separated into low (0 to 0.75 ppbv), medium (0.75 to 1.5 ppbv), and high (> 1.5 ppbv) ambient MT concentration ranges. The inset shows the correlation ($R^2 = 0.47$) between the LVOC fate corrected maximum OA enhancement (0.4–1.5 eq. days aging) and in-canopy MT concentrations.

30466

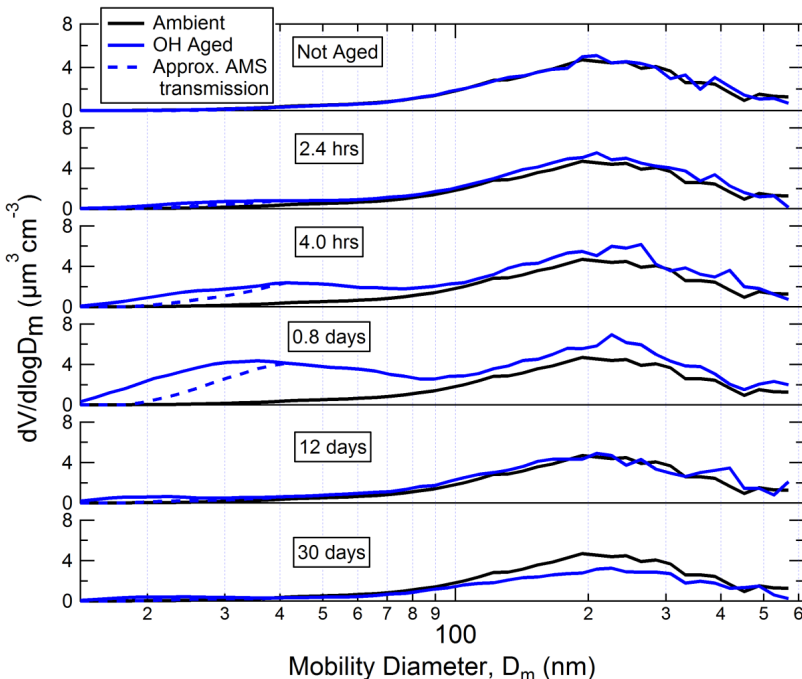


Figure 9. SMPS volume size distributions after OH oxidation using the OFR185 method, labeled by photochemical age and compared to concurrent ambient measurements. Each of the 6 OH-aged size distributions is an average of 6 SMPS scans from the night of 28–29 July, when relatively large OA enhancement was observed and the ambient aerosol surface area was in the range of $80\text{--}100 \mu\text{m cm}^{-3}$. Dashed lines represent the approximate size distributions that were transmitted through the AMS aerodynamic lens (for which a correction was applied to reported OA values as discussed in Sect. S3). Scans with large OA enhancement were used in order to more clearly illustrate the condensation vs. nucleation behavior in the OFR, so the AMS lens transmission correction in this figure appears larger than average. All scans have been corrected for small particle losses to sampling lines (Sect. S1).

In situ secondary organic aerosol formation from ambient pine forest air

B. B. Palm et al.

Title Page

Abstract

Introduction

Conclusions

References

Tables

Figures

| <

Back

Close

Full Screen / Esc

[Printer-friendly Version](#)

Interactive Discussion

In situ secondary organic aerosol formation from ambient pine forest air

B. B. Palm et al.

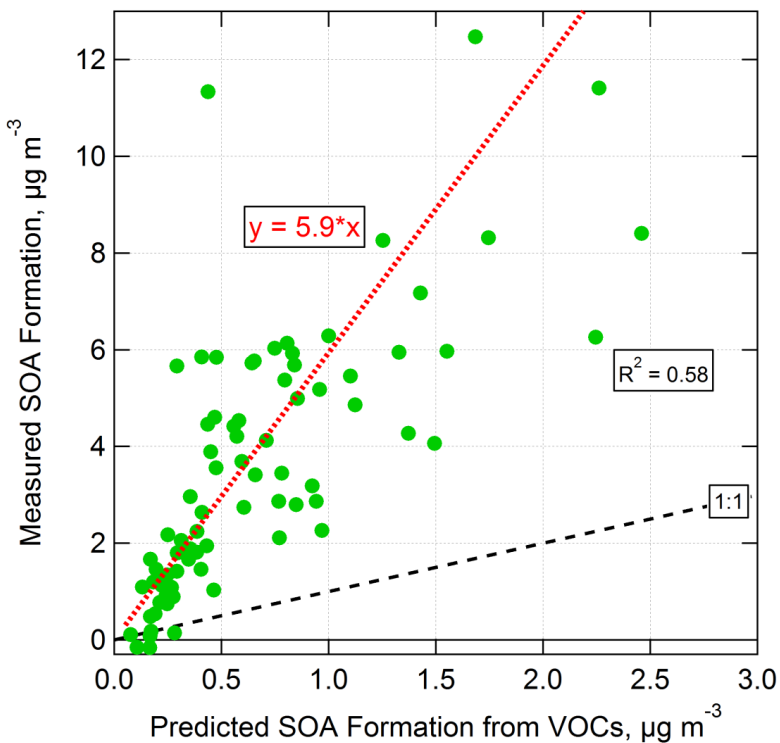


Figure 10. Measured vs. predicted SOA formation from OH oxidation of ambient air in an OFR using the OFR185 method. Only the range of photochemical ages with the highest SOA formation (0.4–1.5 eq. days) was used, and the LVOC fate correction was applied. Predicted SOA formation was calculated by applying OA concentration-dependent yields (average of 13.3, 14.9, 15.9, and 1.8 % for MT, SQT, toluene + *p*-cymene, and isoprene, respectively, with average OA concentration of $5.1 \mu\text{g m}^{-3}$) to VOCs reacted in the OFR (Tsimpidi et al., 2010). The amount of reacted VOCs was estimated using OH_{exp} and ambient VOC concentrations. If a non-zero y intercept is allowed, the regression line becomes $y = 7.0x - 1.0$.

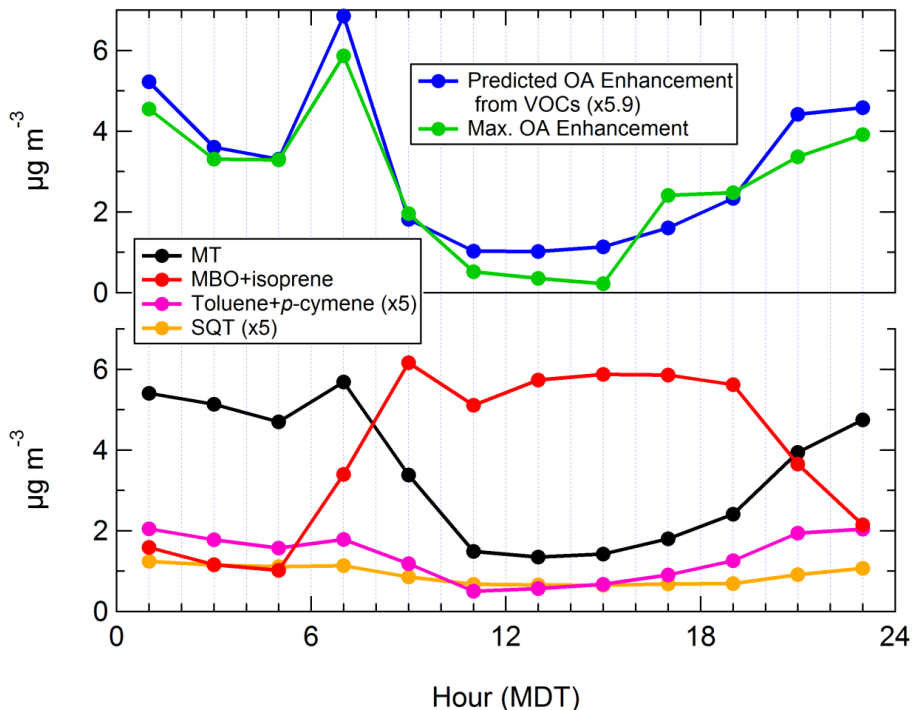


Figure 11. Top: diurnal maximum measured OA enhancement (all data from 0.4–1.5 eq. days aging, LVOC fate corrected) in the OFR from OH oxidation using the OFR185 method, and predicted OA formation from measured VOCs ($\times 5.9$). Bottom: ambient MT, SQT ($\times 5$), toluene + *p*-cymene ($\times 5$), and MBO + isoprene concentrations vs. time of day.

In situ secondary organic aerosol formation from ambient pine forest air

B. B. Palm et al.

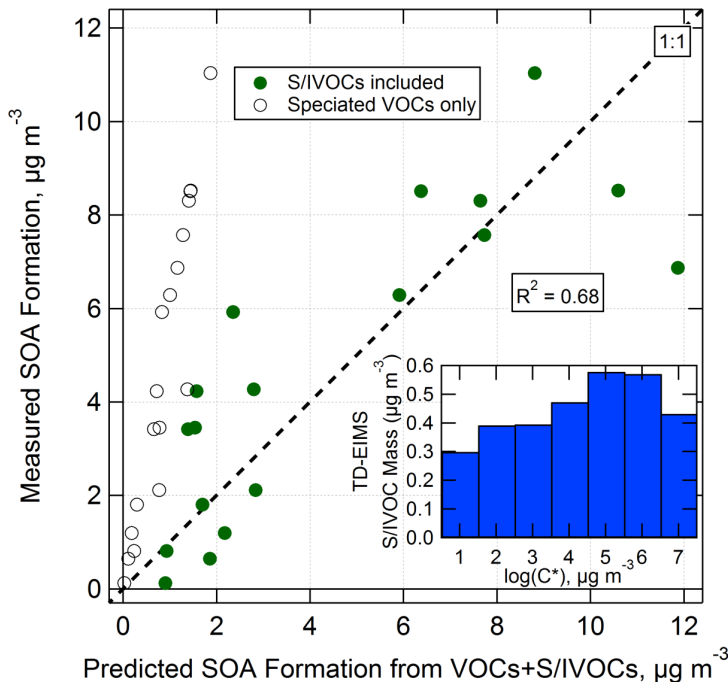


Figure 12. Measured vs. predicted SOA formation from OH oxidation of ambient air in an OFR using the OFR185 method. Only the range of photochemical ages with the highest SOA formation (0.4–1.5 eq. days) was used, and the LVOC fate correction was applied. Predicted SOA formation is estimated using VOCs (described in Sect. 3.6.1) with and without including an empirical 80 % SOA yield from S/I VOCs measured by the TD-EIMS (a lower limit of total S/I VOCs). Inset: average S/I VOC concentrations as a function of the log of the saturation vapor concentration C^* . This comparison includes all data for which S/I VOCs and SOA formation in the OFR were concurrently measured (26, 28–29 July, and 9–10, 12–13 August). For some data points, PTR-TOF-MS data was not available, so the VOC contribution was estimated using the linear fit in Fig. 10.

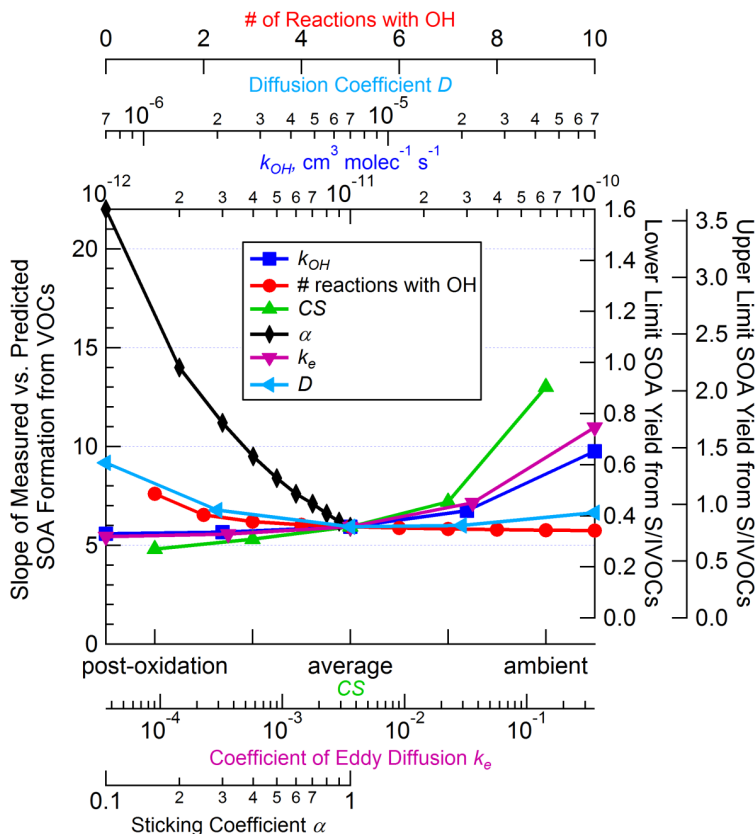


Figure 13. Sensitivity of the slope of measured vs. predicted SOA formation from VOCs, and of the range of SOA yields estimated for bulk S/I VOCs (same curves, different y axes), to parameters in the LVOC fate model. The change in slope and yields is calculated by changing only one parameter at a time while keeping the rest at the base case values of 5 reactions with OH, $k_{\text{OH}} = 1 \times 10^{-11} \text{ cm}^3 \text{ molec}^{-1} \text{ s}^{-1}$, average CS, $\alpha = 1$, $k_e = 0.0036 \text{ s}^{-1}$, and $D = 7 \times 10^{-6} \text{ m}^2 \text{ s}^{-1}$.

In situ secondary organic aerosol formation from ambient pine forest air

B. B. Palm et al.

Title Page

Abstract

Introduction

Conclusio

References

Tables

Figures

Back

Close

Full Screen / Esc

[Printer-friendly Version](#)

Interactive Discussion